Pharmacological Dissection and Distribution of NaN/Nav1.9, T-type Ca^{2+} Currents, and Mechanically Activated Cation Currents in Different Populations of DRG Neurons

Bertrand Coste, Marcel Crest, and Patrick Delmas

Laboratoire de Neurophysiologie Cellulaire, Centre National de la Recherche Scientifique, UMR 6150, Faculté de Médecine, IFR Jean Roche, 13916 Marseille Cedex 20, France

Low voltage–activated (LVA) T-type Ca^{2+} ($I_{Ca}T$) and NaN/Nav1.9 currents regulate DRG neurons by setting the threshold for the action potential. Although alterations in these channels have been implicated in a variety of pathological pain states, their roles in processing sensory information remain poorly understood. Here, we carried out a detailed characterization of LVA currents in DRG neurons by using a method for better separation of NaN/Nav1.9 and $I_{Ca}T$ currents. NaN/Nav1.9 was inhibited by inorganic I_{Ca} blockers as follows (IC_{50}, μM): La^{3+} (46) > Cd^{2+} (233) > Ni^{2+} (892) and by mibefradil, a non-dihydropyridine $I_{Ca}T$ antagonist. Amiloride, however, a preferential Cav3.2 channel blocker, had no effects on NaN/Nav1.9 current. Using these discriminative tools, we showed that NaN/Nav1.9, Cav3.2, and amiloride- and Ni^{2+}-resistant $I_{Ca}T$ (AR-$I_{Ca}T$) contribute differentially to LVA currents in distinct sensory cell populations. NaN/Nav1.9 carried LVA currents into type-I (*CI*) and type-II (*CII*) small nociceptors and medium-Aδ–like nociceptive cells but not in low-threshold mechanoreceptors, including putative Down-hair (D-hair) and Aα/β cells. Cav3.2 predominated in *CII*-nociceptors and in putative D-hair cells. AR-$I_{Ca}T$ was restricted to *CII*-nociceptors, putative D-hair cells, and Aα/β-like cells. These cell types distinguished by their current-signature displayed different types of mechanosensitive channels. *CI*- and *CII*-nociceptors displayed amiloride-sensitive high-threshold mechanical currents with slow or no adaptation, respectively. Putative D-hair and Aα/β-like cells had low-threshold mechanical currents, which were distinguished by their adapting kinetics and sensitivity to amiloride. Thus, subspecialized DRG cells express specific combinations of LVA and mechanosensitive channels, which are likely to play a key role in shaping responses of DRG neurons transmitting different sensory modalities.

INTRODUCTION

Dorsal root ganglia (DRG) neurons form a heterogeneous population based on criteria such as cell body size, structures innervated, and sensory modalities. During the last 20 years, compelling evidence has accumulated that suggests that these physiologically and anatomically distinct populations of DRG neurons also express different subsets of ion channels (Waxman et al., 1999; Wood et al., 2004; Wang and Woolf, 2005).

Based on their differential sensitivity to tetrodotoxin (TTX), Na^+ channels are typically classified into TTX-sensitive and TTX-resistant subunits. Small- to medium-sized DRG neurons express TTX-resistant Na^+ currents produced by Nav1.8 and Nav1.9 channel isoforms (Akopian et al., 1996; Sangameswaran et al., 1996; Dib-Hajj et al., 1998; Tate et al., 1998; Benn et al., 2001; Fang et al., 2002). Nav1.8 encodes a slowly activating and inactivating current (also known as SNS or PN3), which has a relatively depolarized threshold for activation and may support action potential propagation in C- and Aδ-nociceptive fibers (Akopian et al., 1996; Sangameswaran et al., 1996; Blair and Bean, 2002). In contrast, the Nav1.9 subunit (also known as NaN or SNS2) generates a low voltage–activated (LVA) channel current with very slow activation and inactivation rates and larger single channel conductance (Herzog et al., 2001; Coste et al., 2004). Nav1.9 channels give rise to a "persistent" Na^+ current at subthreshold voltages that lowers action potential threshold and promotes burst discharges (Herzog et al., 2001; Baker et al., 2003; Coste et al., 2004). Mice with nonfunctional Nav1.9 channels do not develop the persistent heat hyperalgesia that is normally seen in inflammatory pain models (Priest et al., 2005).

In addition to Nav1.9 channels, DRG neurons also express LVA T-type Ca^{2+} currents ($I_{Ca}T$) (Carbone and Lux, 1984; Bossu et al., 1985; Nowycky et al., 1985; Scroggs and Fox, 1992; Shin et al., 2003). These channels are activated by weak depolarizations near resting potential and act as efficient tuners of cell excitability (Huguenard, 1996). The pivotal role of $I_{Ca}T$ in nociception has been inferred previously (Dogrul et al., 2003) and recently confirmed by antisense knocking-down strategies (Bourinet et al., 2005).

Correspondence to Patrick Delmas: delmas.p@jean-roche.univ-mrs.fr

Abbreviations used in this paper: D-hair, Down-hair; DRG, dorsal root ganglia; HVA, high voltage–activated; $I_{Ca}T$, LVA T-type Ca^{2+} currents; LVA, low voltage–activated; TTX, tetrodotoxin.

J. Gen. Physiol. © The Rockefeller University Press $15.00
Volume 129 Number 1 January 2007 57–77
http://www.jgp.org/cgi/doi/10.1085/jgp.200609665

Supplemental material can be found at:
http://doi.org/10.1085/jgp.200609665

Given that the expression of LVA currents has a unique impact on neuronal excitability, it is of great interest to know which DRG cell subpopulations express a combination of NaN/Nav1.9 and $I_{Ca}T$ channels. Using pharmacological discriminating tools, we have broken down LVA currents and provided a thorough description of the specific contribution of NaN/Nav1.9 and $I_{Ca}T$ complements in over 350 DRG neurons. To better characterize DRG cell subpopulations, we combined this approach with the measurement of cell size, capsaicin sensitivity, and characterization of mechanically activated cation currents. Reliance on identification of DRG cell populations from the presence of these different channels has the potential to provide criteria by which nociceptive and nonnociceptive subpopulations might be distinguished. Based on these current signatures, DRG cells were classified into five main, internally uniform subgroups, each expressing a unique combination of LVA and sensory channels. Our study therefore provides a characteristic fingerprint of LVA-channels' activity in DRG nociceptors and mechanoreceptors, which may aid in the understanding of their physiological function.

MATERIALS AND METHODS

DRG Cell Cultures

Young rats (male Wistars, 120–130 g) were anesthetized with halothane and killed by severing of the carotid arteries in accordance with the Guide for the Care and Use of Laboratory Animals. Cultures of DRG neurons were established from thoraco-lumbar DRGs excised and freed from their connective tissue sheaths. They were incubated in enzyme solution containing 2 mg/ml of collagenase IA (GIBCO BRL) for 45 min at 37°C and triturated in Hanks' medium (GIBCO BRL). The resulting suspension was plated in Nunclon dishes. Culture medium was Dulbecco's modified Eagle's medium (DMEM) supplemented with 10% heat-inactivated FCS, 100 U/ml penicillin-streptomycin, 2 mM L-glutamine, 25 ng/ml nerve growth factor (NGF), and 2 ng/ml glial-derived neurotrophic factor (GDNF) (all from GIBCO BRL). Neurons were recorded within 4–12 h after plating. Care and use of rats were in accordance with institutional guidelines.

Whole-Cell Patch-Clamp Recording

Patch pipettes had resistance of 2–3 MΩ when filled with an internal solution consisting of (in mM) 100 CsCl, 30 CsF, 10 HEPES, 10 EGTA, 8 NaCl, 1 $CaCl_2$, 1 $MgCl_2$, 4 MgATP, and 0.4 Na_2GTP (pH adjusted to 7.3, 304 mOsm). In some recordings of large DRG neurons, CsF was substituted by CsCl. The use of internal fluoride facilitates inhibition of high voltage–activated (HVA) Ca^{2+} currents (Kostyuk et al., 1975; Akaike et al., 1989; Herrington and Lingle, 1992; Todorovic and Lingle, 1998) and helps to reveal NaN/Nav1.9 currents (Coste et al., 2004; Maruyama et al., 2004). Thus, for all experiments, once the whole-cell configuration had been attained, currents were allowed to stabilize for ∼5 min before beginning recordings. Cells for which currents continued to fluctuate after this time were not recorded further.

The extracellular solution consisted of (in mM) 60 NaCl, 110 sucrose, 3 KCl, 1 $MgCl_2$, 10 HEPES, 2.5 $CaCl_2$, 10 glucose, 10 TEA-Cl, 0.0005 TTX (pH 7.3, 296 mOsm). The "low sodium" external solution was achieved by isoosmotically substituting NaCl by sucrose but still contained 2 mM Na^+. This was done to prevent changes in intracellular [Ca^{2+}] that might result from the reversing of the Na^+/Ca^{2+} exchanger. Whole-cell currents were measured with an Axopatch 200B amplifier (Axon Instruments Inc.), filtered at 1–2 kHz (four-pole Bessel filter), and sampled at a rate five times the filter frequency. Otherwise noticed, currents were leak subtracted using a P/6 protocol as previously described (Delmas et al., 2000; Coste et al., 2004). Voltage errors were minimized using 70–85% series resistance compensation. The access resistance ranged between 4 and 7 MΩ. Cell capacitance was estimated from the time constant of the decay phase of a current transient elicited by a 10-mV hyperpolarizing step from a holding potential of −100 mV. All experiments were done at room temperature.

Mechanical Stimulation

After electrophysiological characterization of DRG neurons in whole-cell recording mode, the cell was subjected to incremental mechanical stimulation. Mechanical stimulation was achieved using a fire-polished glass pipette (tip diameter 3–4 μm) positioned at an angle of 60° to the cell being recorded. Downward movement of the probe toward the cell was driven by a PClamp-controlled piezo-electric crystal microstage (Step Driver PZ-100; Burleigh). The probe was typically positioned 2 μm from the cell body. This distance probe-cell was then subtracted from the total distance travelled by the probe, thereby defining the actual stimulus intensity. The probe had a velocity of 200 μm/s during the ramp segment of the command for forward motion and the stimulus was applied for 100–200 ms. To assess the mechanical sensitivity of a cell, a series of mechanical steps in 1–2-μm increments were applied every 15 s, which allowed full recovery of most mechanosensitive currents.

Cell Classification

Our approach to neuronal identification of rat DRG neurons draws on previous studies (Cardenas et al., 1995; Djouhri et al., 1998; Petruska et al., 2000; Petruska et al., 2002). Although the association between DRG cell classes in vitro and in vivo remains speculative, our classification scheme was based on the notion that functionally uniform cell populations can be identified by their repertoire of ion channels. Cells were classified according to five cluster variables, namely, peak amplitude (normalized for cell size, pA/pF) of NaN/Nav1.9, SNS/Nav1.8, amiloride-sensitive and amiloride-resistant $I_{Ca}T$, and cell capacitance (pF). For clustering, we used a nonhierarchical method based on a K-means algorithm (Anderberg, 1973) and a Euclidean distance measure was used to calculate how close each cell is to the target group. The analysis was repeated for a number of clusters varying from 1 to 15, and the optimal number of clusters was determined using the cubic clustering criterion statistics. Based on these cluster variables, five groups of cells could be classified into distinct, but internally homogeneous, subpopulations. To determine whether these groups had predictive validity, we examined whether each cell cluster was homogeneous with respect to sensory modalities, including properties of mechanosensitive currents and responsiveness to capsaicin. To obtain the entire battery of characteristics, we recorded cells for ∼60–90 min. Note that the presence of other, mostly heterogeneous, groups of DRG cells (∼15% of the total sampling) suggests the existence of additional types of neurons that occur less frequently. Because of the paucity of data on these cells, they were not included in this study.

The DRG cells from which we recorded had properties consistent with nociceptors, Down-hair (D-hair) cells, and Aα/β cells. Cells classified as nociceptors have small (C-type, 14–40 pF) or medium (Aδ-type, 35–70 pF) diameters, are sensitive to capsaicin, and/or express Nav1.9/NaN current (Fang et al., 2002; 2006). D-hair cells have medium size (39–65 pF) and very distinctive

$I_{Ca}T$ (Shin et al., 2003; Dubreuil et al., 2004), whereas Aα/β cells have large diameters (70–105 pF).

Drug Application and Chemicals

Extracellular media were exchanged using a gravity-fed bath perfusion system at a flow rate of 10 ml/min, while bath solution was removed by continuous suction. The volume of fluid in the recording chamber was 1 ml, allowing the exchange of bathing solution within 6–8 s. Recycling was used to reduce the amount of TTX used. Block of currents, irrespective of the channel types examined, was estimated as inhibition of peak currents during 100-ms test pulses from a holding potential of −100 mV at a frequency of 0.2–0.33 Hz. For concentration–response studies, increasing concentrations of blockers were applied sequentially while stimulation of the cell was continued at 0.2–0.33 Hz until the response for a given concentration reached a plateau. This procedure was performed 5–8 min from rupturing the patch before any rundown of NaN/Nav1.9 current could occur. SNS/Nav1.8 and $I_{Ca}T$ were not susceptible to substantial rundown.

All chemicals were obtained from Sigma-Aldrich, except TTX (Alomone Labs). Stock solutions of TTX (0.1 mM), mibefradil (5 mM), Ni^{2+}, La^{3+}, and Cd^{2+} (100 mM) were prepared in water. A stock solution of 1 M amiloride was made by dissolving amiloride hydrochloride in DMSO. The maximum concentration of DMSO in the superfusate for these experiments was 0.3%, which was determined to have no effects on DRG currents in control experiments. A stock solution of 50 mM capsaicin was prepared in 100% ethanol. The maximum concentration of ethanol in the superfusate was 0.002%, which had no apparent effects on current properties. Our attempt to reduce external Ca^{2+} ion concentrations to ∼0–10 μM (while increasing Mg^{2+} to 5–8 mM) in order to suppress Ca^{2+} currents led to seal instability and made DRG cells unhealthy (see also Rush et al., 1998). This made routine experiments with nominally Ca^{2+}-free solutions virtually impossible, especially because more than 1–2 h recording was typically required in order to characterize electrophysiologically and pharmacologically the cells under investigation.

Data and Statistical Analysis

PCLAMP 8.02 (Axon Instruments Inc.) and PRISM 4.0 (GraphPad) software suites were used to perform linear and nonlinear fitting of data. We refer to LVA currents as currents activating at voltages more negative than −55 mV. Current density of NaN/Nav1.9 was measured between −55 and −65 mV where SNS/Nav1.8 was absent. Amplitude of SNS/Nav1.8 current was estimated using a 2-s conditioning prepulse to −50 mV before test depolarization, to inactivate the NaN/Nav1.9 current, leaving the SNS/Nav1.8 current almost intact (Cummins et al., 1999). Conductance–voltage curves were calculated from the peak current according to the equation $G = I/(V - E_{rev})$, where V is the test pulse potential and E_{rev} the reversal potential calculated according to the Nernst equation. The activation curve (G-V) was fitted using the Boltzmann function: $G/G_{max} = 1/(1 + \exp[(V_{1/2} - V)/k])$, where G/G_{max} is the normalized conductance, $V_{1/2}$ is the potential of half-maximum channel activation, and k is the steepness factor. NaN/Nav1.9 *I-V* curves were fitted with a curve according to: $I_{NaN}(V) = G_{max}(V - E_{rev})/\{1 + \exp[(V_{1/2} - V)/k]\}$, where $I_{NaN}(V)$ is the peak current in response to the test depolarizing potential. The time courses of inactivation and tail currents were fitted to exponentials using the Chebyshev nonlinear least-square fitting procedure. The concentration–inhibition curves for channel blockers were fitted with the Hill equation of the form $Y = Y_{max}[blocker]^{nH}/(IC_{50}{}^{nH} + [blocker]^{nH})$, where Y is the percentage inhibition (e.g., $100 * I/I_{[blocker]=0}$), IC_{50} the blocker concentration that produces half-maximal inhibition, and n_H the Hill coefficient. Results are presented as mean ± SEM (or mean ± SD when indicated), and *n* represents the number of cells examined. Statistical comparisons were analyzed using Student's *t* test or ANOVA. $P < 0.05$ was considered statistically significant.

Online Supplemental Material

Fig. S1 (available online at http://www.jgp.org/cgi/content/full/jgp.200609665/DC1) shows the effect of amiloride on SNS/Nav1.8 and NaN/Nav1.9 currents in the presence of 30 μM La^{3+} (to block Ca^{2+} currents). Voltage-clamp whole-cell recordings were made using the CsF-based internal solution as described in the whole-cell patch-clamp recording method section.

RESULTS

Heterogeneity of LVA Currents in DRG Neurons As Revealed by Variable Sensitivities to Cadmium

Low voltage–activated (LVA) inward currents were studied from 367 cells of acutely dissociated rat DRGs, using physiological Ca^{2+} concentrations ($[Ca^{2+}]_o$ = 2.5 mM) and reduced driving force for Na^+ ($[Na^+]_o$ = 60 mM). Under these conditions, the neurons were electrically compact and amenable to careful voltage-clamp. With TTX (500 nM) in the bathing solution, depolarizing pulses from a holding potential of −100 mV evoked LVA inward currents in the vast majority (338 out of 367) of neurons recorded irrespective of their cell body diameter. Fig. 1 A gives examples of LVA currents recorded in four different DRG neurons, which activated roughly between −80 and −70 mV and were distinguishable at first glance by their inactivation kinetics. Fig. 1 A (a and d) shows uniform slowly activating LVA currents with either very modest or almost complete inactivation during 100-ms step depolarization, respectively. These two samples represent prototypical LVA currents, which we predict to be mediated by NaN/Nav1.9 (Fig. 1 A, a) and T-type Ca^{2+} channels (Fig. 1 A, d).

However, in most small- and medium-sized DRG neurons, LVA currents were more complex, exhibiting more or less pronounced inactivation. Hereafter we refer to these currents as mixed-LVA currents, with the presumption that they are generated by different classes of channels. Fig. 1 A (b and c) illustrates two of such LVA currents in small-diameter DRG neurons (25 and 21 pF, respectively), which had very similar thresholds of activation but distinct inactivation kinetics. We postulated that these mixed kinetics of inactivation might reflect differential contribution of Ca^{2+} and Na^+ components to LVA currents. Because Ca^{2+} current components could not be eliminated using Ca^{2+}-free bathing solutions due to experimental instability (see Materials and methods), we first attempted to dissect LVA currents using cadmium (Cd^{2+}), a nonselective Ca^{2+} channel blocker. Classically, Cd^{2+} ions are considered to preferentially block Ca^{2+} channels over Na^+ channels. However, there is now good evidence that Cd^{2+} is also a blocker of TTX-R Na^+ currents (Visentin et al., 1990; Backx et al., 1992; Sheets and Hanck, 1992; Kuo et al., 2002; Leffler et al., 2005).

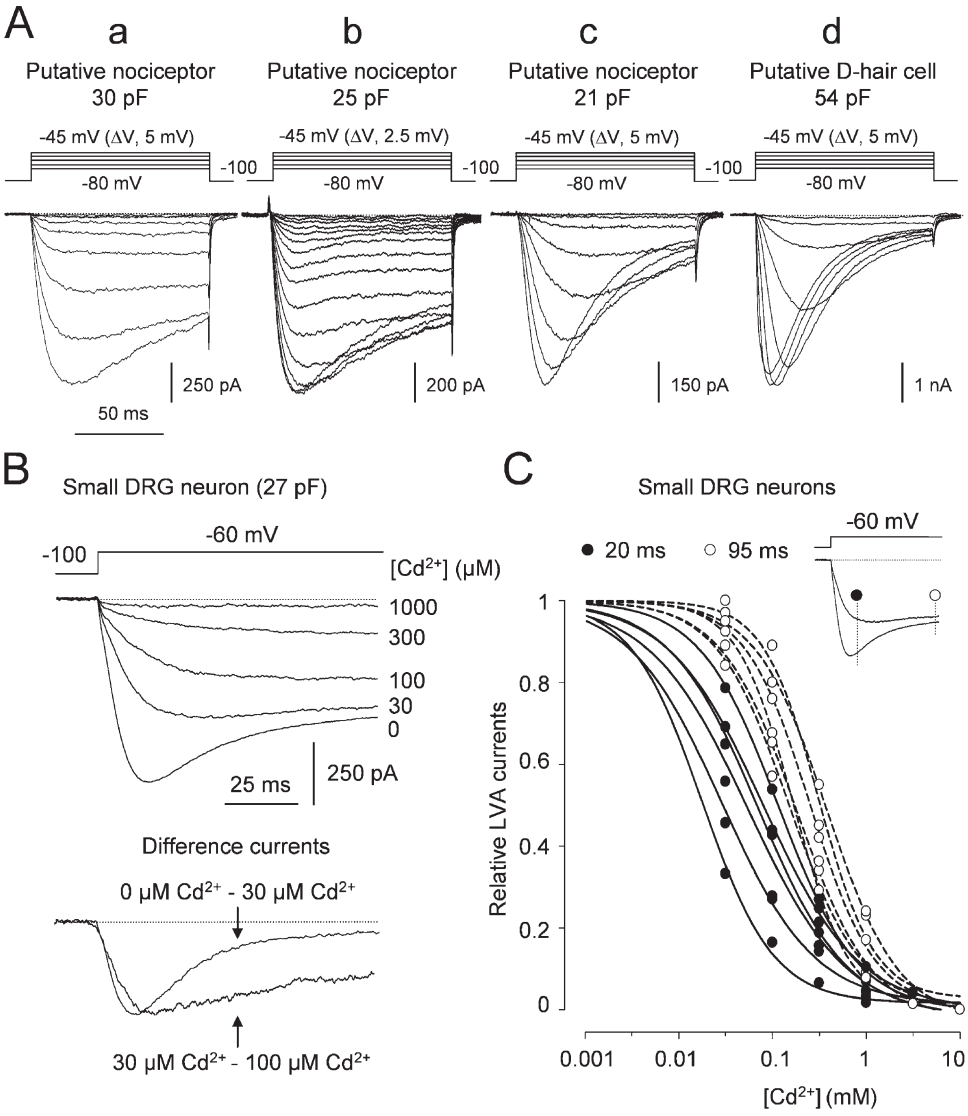

Figure 1. Heterogeneity of low-threshold inward currents in DRG neurons. (A) Families of current traces elicited in small- (a–c) and medium- (d) diameter DRG neurons by 100-ms depolarizations. Currents were evoked by stepping from −80 to −45 mV in 2.5- or 5-mV increments from a holding potential of −100 mV. Note the difference in inactivation kinetics of these LVA currents. Membrane capacitance is indicated for each cell. (B) Block of mixed LVA current by increasing concentrations of Cd^{2+} (0–1000 μM, as indicated) in a small DRG neuron (27 pF). The bottom panel shows peak-normalized difference currents determined as indicated. (C) Cadmium block of mixed LVA currents in small-sized DRG neurons (15–29 pF, $n = 6$) determined isochronally 20 or 95 ms after the onset of the test pulse (inset). Data were obtained with a 100-ms test pulse to −60 mV from a holding potential of −100 mV once every 5 s and normalized to current amplitude obtained before application of drug. Data points were plotted against $[Cd^{2+}]$ in semilogarithmic scale and best fit to single site binding curves (solid and dashed lines). IC_{50} ranged from 13 to 200 μM (n_H = 0.8–1.56) and from 149 to 381 μM (n_H = 1.05–1.2) when determined at t = 20 and t = 95 ms, respectively. Mean IC_{50} values obtained at t = 20 and t = 95 ms were 44 ± 11 and 240 ± 35 μM, which were significantly different ($P < 0.005$; two-tailed unpaired t test).

Effects of Cd^{2+} on a sample mixed-LVA current evoked by a step depolarization to −60 mV in a small DRG neuron is shown in Fig. 1 B. External Cd^{2+} reduced the peak LVA current in a dose-dependent fashion, with marked effects on both the timing of the peak current and the decaying kinetics of the current. Isolation of LVA current components blocked by Cd^{2+} shows that low concentrations of Cd^{2+} (30 μM) preferentially abolished a rapidly inactivating current, while slightly higher concentrations suppressed a "persistent" current. These findings may be explained if the total LVA current were comprised of multiple components, showing different sensitivity to Cd^{2+} and distinct inactivating time course. This heterogeneity is further illustrated in Fig. 1 C, which depicts the concentration dependency of Cd^{2+} block of LVA currents in small- sized DRG neurons demonstrating mixed kinetics. Cd^{2+} was able to produce total inhibition of LVA currents measured isochronally at 20 ms, although with variable potencies. This large variation in IC_{50} from 17 to 200 μM and Hill coefficients from 0.8 to 1.56 clearly indicated some deviation from one-to-one binding curves in most cells, suggestive of channel heterogeneity (e.g., multiple Cd^{2+} binding sites). To confirm that Cd^{2+} inhibited distinct LVA current components with different inactivation kinetics, plot of the relative current against Cd^{2+} concentration was determined isochronally at 95 ms after the onset of the test pulse, where "persistent" currents predominate. Using this procedure, data points could be reasonably well fitted by a one-to-one binding curve, giving IC_{50} ranging from 149 to 381 μM and cooperativity coefficients ranging from 1.05 to 1.2 (Fig. 1 C, ○). These observations

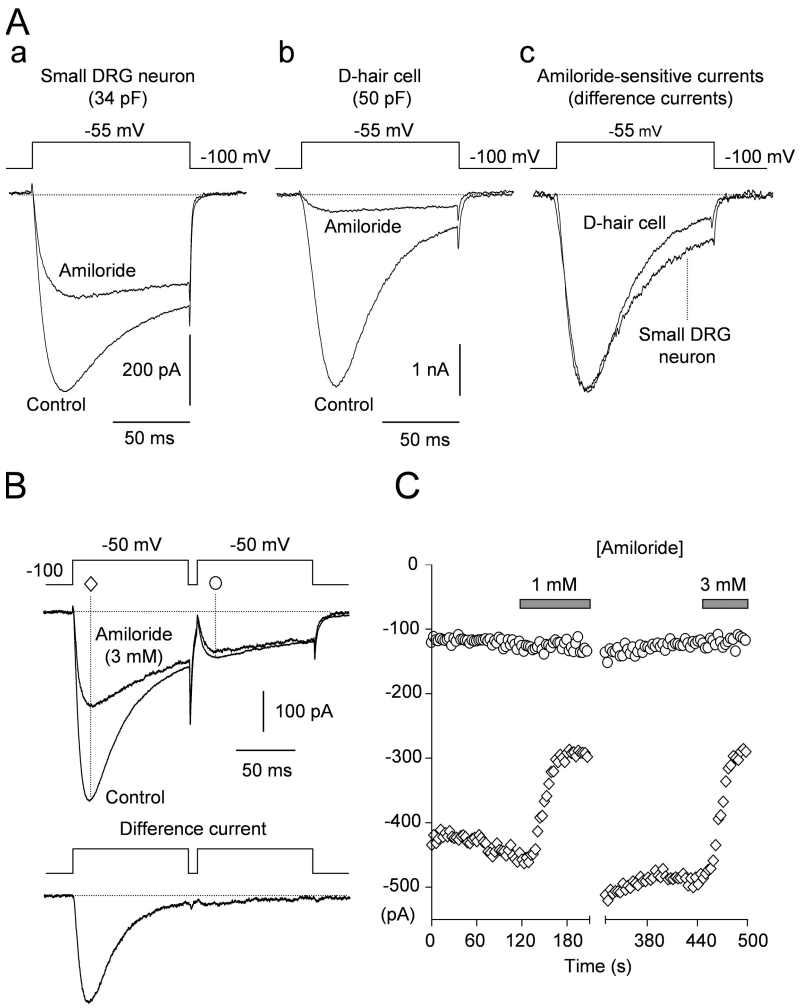

Figure 2. Amiloride blocks low-threshold T-type Ca^{2+} current but spares NaN/Nav1.9 current. (A) Inhibition of LVA currents by amiloride (1 mM) in a small DRG neuron (34 pF, a) and in a medium-diameter D-hair cell (50 pF, b). Currents were evoked by a depolarizing step to −55 mV from a holding of −100 mV and amiloride inhibition is shown at steady state. (A, c) Superimposed amiloride-sensitive LVA currents (difference currents) obtained in the corresponding small- and medium-diameter DRG neurons as indicated. Traces are scaled for comparison. (B) LVA currents evoked by a double-pulse voltage protocol in the absence and presence of 3 mM amiloride in a small DRG neuron (23 pF). The voltage protocol consisted of two 100-ms depolarizing steps to −50 mV, separated by a 4-ms interpulse to −100 mV, which was short enough to prevent repriming of T-type Ca^{2+} channels. (C) Amplitude of LVA currents plotted as a function of time for the corresponding cell shown in B. The horizontal bars indicate the time and duration of application of amiloride. The DRG neuron was stimulated every 3 s by the use of the double-pulse protocol as in B.

prompted us to suggest that the inactivating component of LVA currents with the higher sensitivity to Cd^{2+} reflects the contribution of $I_{Ca}T$, whereas the persistent component, which appeared to be slightly less sensitive to Cd^{2+}, is likely to arise from NaN/Nav1.9 channels.

Amiloride Blocks T-type Ca^{2+} Currents but Not NaN/Nav1.9 Current

Because NaN/Nav1.9 and $I_{Ca}T$ cannot be distinguished by their sensitivity to cadmium, we examined some organic agents reported to be effective in inhibiting $I_{Ca}T$ and that act via a locus independent of the metal cation binding site. One of these agents is the pyrazinecarboxamide diuretic amiloride, which was reported to potently inhibit $I_{Ca}T$ in various systems (Fox et al., 1987; Tang et al., 1988; Scroggs and Fox, 1992; Todorovic and Lingle, 1998). Fig. 2 A illustrates the effects of 1 mM amiloride on LVA currents evoked at −55 mV (a voltage at which SNS/Nav1.8 is absent) in both small- and medium-sized DRG neurons. The 1 mM amiloride concentration blocked about half of the mixed-LVA current in the small DRG neuron. Only the component of peak current with fast inactivation, which could be attributable to $I_{Ca}T$, was suppressed by amiloride, leaving the steady-state current, attributable to NaN/Nav1.9, largely unchanged (measured at T = 95 ms). These effects were observed in additional 49 small-sized DRG neurons. The digitally subtracted amiloride-sensitive currents in small DRG neurons had kinetics similar to those blocked by amiloride in medium diameter putative D-hair cells, in which large $I_{Ca}T$, recently identified as Cav3.2, predominates (Shin et al., 2003; Dubreuil et al., 2004) (Fig. 2 A, b and c).

The effectiveness and selectivity of amiloride in achieving inhibition of $I_{Ca}T$ but not NaN/Nav1.9 was further tested by comparing effects of amiloride applied successively at 1 and 3 mM (Fig. 2, B and C). In this set of experiments, a two-pulse protocol was used to observe inactivating and persistent LVA currents in relative isolation. An initial prepulse to –50 mV activated mixed-LVA currents, but resulted in complete inactivation of presumptive $I_{Ca}T$, leaving only persistent NaN/Nav1.9 to be available for activation in the closely timed second test pulse. Here again, amiloride blocked the inactivating current component but had negligible effects on the persistent component. The currents in 3 mM amiloride

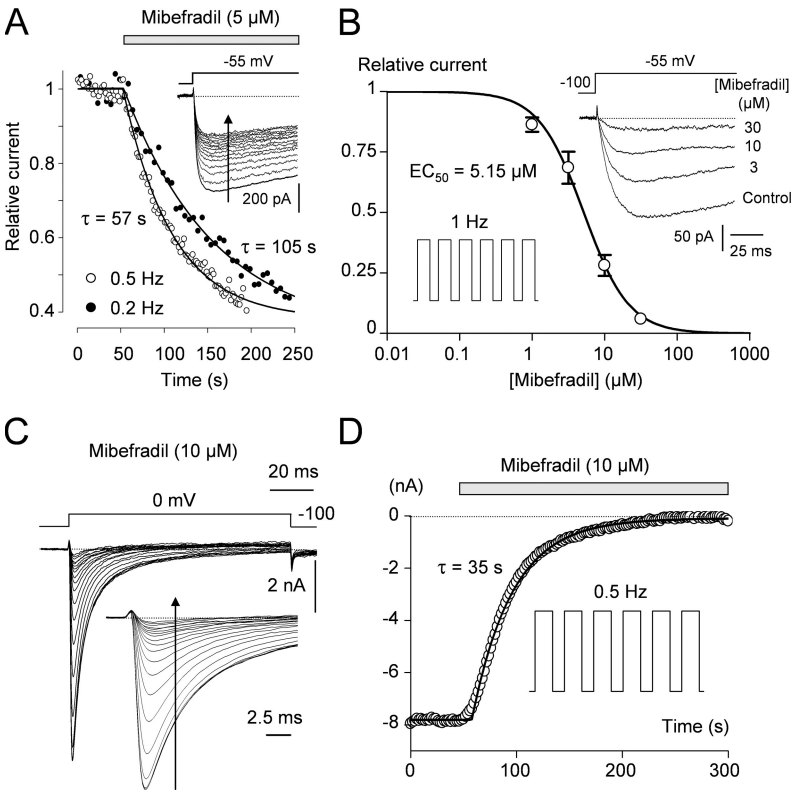

Figure 3. Mibefradil block of NaN/Nav1.9 and SNS/Nav1.8 currents in small DRG neurons. (A) Inhibition of normalized NaN/Nav1.9 current by mibefradil (5 μM) in small DRG neurons. The cells were held at −100 mV and depolarized to −55 mV at 0.2 (●) or 0.5 Hz (○). Smooth curves show single exponential fits with time constants as indicated. Insert shows mibefradil inhibition of NaN/Nav1.9 current evoked at 0.5 Hz; for clarity's sake, only 1 trace every 10 s is shown. Mean time constants for mibefradil block were 49 ± 6 and 112 ± 7 s at 0.5 and 0.2 Hz, respectively ($n = 6$; $P < 0.05$). (B) Concentration–inhibition curve for mibefradil in small DRG neurons (18–27 pF). Mibefradil was cumulatively applied at increasing concentrations (1–30 μM) for the time necessary to approach equilibrium at 1 Hz. Hill equation was used to fit data and yielded an IC_{50} value of 5.15 ± 0.5 μM ($n_H = 1.2$). Each data point is the mean ± SEM of 11 observations. The insert shows superimposed NaN/Nav1.9 current in the absence or presence of increasing concentrations of mibefradil (3–30 μM). (C) Inhibition of SNS/Nav1.8 current by 10 μM mibefradil in a small DRG neuron (29 pF) in which SNS/Nav1.8 predominates. Currents were evoked by depolarizing voltage steps to 0 mV from a holding potential of −100 mV once every 2 s (0.5 Hz). For clarity, only one trace every 10 s is shown. Inset, expanded time scale. (D) Peak SNS/Nav1.8 current was plotted against time for the corresponding cell in C. All experiments were made in the presence of amiloride (1 mM).

showed no greater degree of block, suggesting that 1 mM amiloride was sufficient to yield a saturating block.

We then explored the effects of amiloride on SNS/Nav1.8 currents recorded in small DRG neurons (22–30 pF) in which SNS was predominant. It was apparent that SNS/Nav1.8 currents were largely insensitive to amiloride. In some instances, SNS/Nav1.8 peak current was slightly decreased by 5–10% by 1 mM amiloride (Fig. S1 A, available at http://www.jgp.org/cgi/content/full/jgp.200609665/DC1). However, this apparent inhibition could be due to a possible contamination arising from block of residual HVA Ca^{2+} currents by amiloride (i.e., not blocked by our F^--containing pipette solution; see Materials and methods). For this reason, subsequent experiments designed to test the sensitivity of SNS/Nav1.8 currents to amiloride were performed in the presence of La^{3+}, one of the most powerful blockers of Ca^{2+} channels. Fig. S1 B shows an experiment in a small-diameter DRG neuron (24 pF) in the presence of 30 μM La^{3+} (i.e., ∼30 times the IC_{50} for most Ca^{2+} channels). Once currents were equilibrated in the La^{3+}-containing solution, subsequent superfusion of amiloride in the continued presence of La^{3+} produced no further block of SNS/Nav1.8 current at 1 mM and ∼20% block at 3 mM (Fig. S1, B and C). Collectively, these data demonstrate that amiloride at 1 mM had negligible effects on TTX-R Na^+ currents.

Pharmacology of NaN/Nav1.9 Current

We next sought to characterize NaN/Nav1.9 currents pharmacologically, using amiloride as a discriminating tool. This analysis was performed in DRG neurons in which only NaN/Nav1.9 current contributed to LVA currents in the presence of amiloride, as tested in each cell by substituting normal external solution with a low Na^+ solution (still containing 2.5 mM Ca^{2+}, which was required for stable long-lasting recordings). We will see below that some DRG cell populations also expressed amiloride-resistant T-type Ca^{2+} currents.

Mibefradil, a Preferential T-type Ca^{2+} Channel Antagonist, Blocks NaN/Nav1.9 as well as Nav1.8 Current

We were also interested in examining the response of NaN/Nav1.9 current to mibefradil, a tetralol derivative chemically distinct from other $I_{Ca}T$ antagonists, which is known to block all three Cav3 channels with equal potency (EC_{50}, 1–3 μM; Martin et al., 2000) and to cause mechanical and thermal antinociception (Todorovic et al., 2002; Dogrul et al., 2003). To study block by mibefradil, we held cells at sufficiently negative potential (V_h = −100 mV) at which a substantial proportion of NaN/Nav1.9 channels were not slow inactivated (Coste et al., 2004). Fig. 3 A shows the effects of mibefradil on the NaN/Nav1.9 current in a small-sized DRG neuron (21 pF) under conditions where $I_{Ca}T$ was blocked by 1 mM

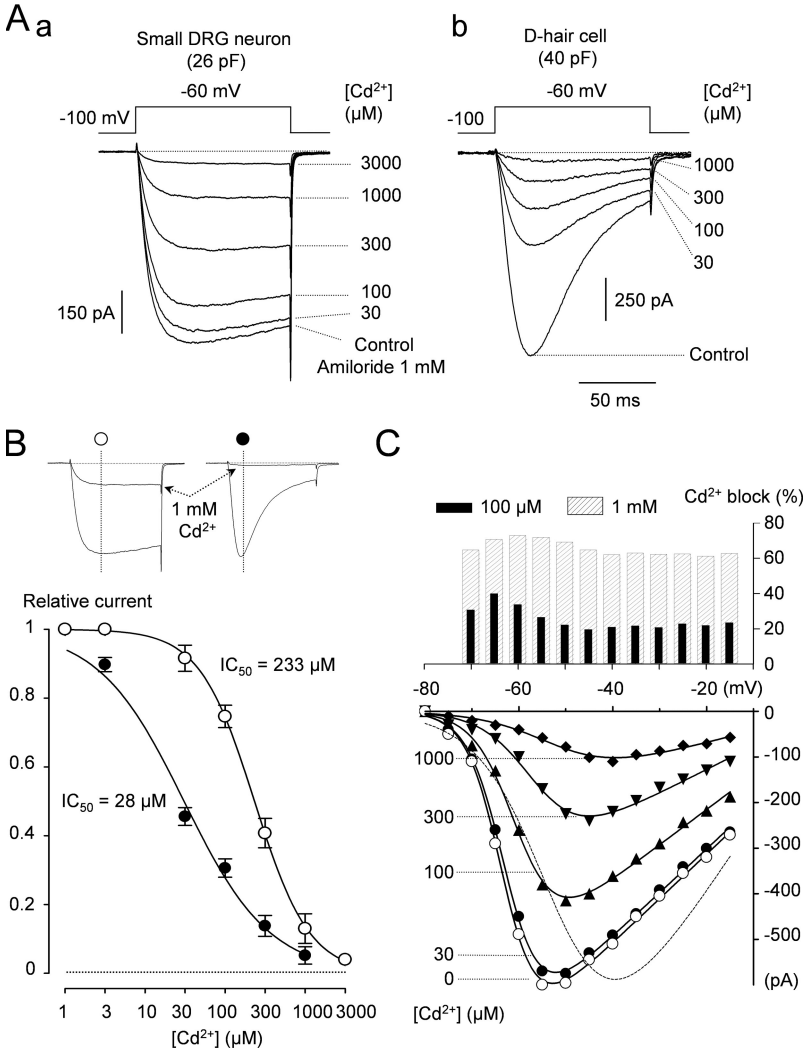

Figure 4. Cadmium block of NaN/Nav1.9 in small DRG neurons. (A) Typical response to increasing concentrations of $CdCl_2$ in a small DRG neuron (26 pF, a) and in a medium-diameter D-hair cell (40 pF, b). Test pulses to −60 mV from a holding potential of −100 mV were delivered every 5 s. Note that amiloride (1 mM) was present throughout in A (a) in order to suppress T-type Ca^{2+} currents. (B) Dose–response analysis of Cd^{2+} block of NaN/Nav1.9 in small DRG neurons (○) and LVA currents (carried primarily by $I_{Ca}T$) in medium-sized D-hair cells (●). Data were obtained with a 100-ms test pulse to −60 mV from a holding potential of −100 mV once every 5 s and normalized to peak current amplitudes measured before application of $CdCl_2$ (inset). Solid lines are the best least-square fits to single binding site equation. Calculated IC_{50} values are 233 ± 5 μM (n_H = 1.1) for NaN/Nav1.9 and 28 ± 2 μM (n_H = 0.81) for $I_{Ca}T$. 8–11 cells per point. (C) Same cell as in A (a). Peak currents were plotted as a function of potential in control condition (0 μM Cd^{2+} + 1 mM amiloride) and in the presence of 30, 100, 300, and 1,000 μM Cd^{2+}, added cumulatively. Smooth curves represent modified Boltzmann fits, giving $V_{1/2}$ and slope factors of −59.5 and 4.5 mV (○), −58.8 and 4.6 mV (●), −56.6 and 4.4 mV (▲), −53.1 and 4.6 mV (▼), and −49 and 6.3 mV (◆). The dashed line represents the data obtained in the presence of 1,000 μM Cd^{2+} normalized to the maximum peak current. Top panel, the percentage block by 100 and 1,000 μM Cd^{2+} was calculated and plotted for each potential.

amiloride. The cell was depolarized to −50 mV, once every 2 or 5 s until current magnitude in mibefradil stabilized. Mibefradil blocked NaN/Nav1.9 channels in a use/frequency-dependent manner, suggesting preferential binding to inactivated state(s), as previously reported by some investigators for other channels (Todorovic and Lingle, 1998; Martin et al., 2000; McNulty and Hanck, 2004). Dose–response curves determined using increasing concentrations of mibefradil in 11 small DRG neurons stimulated at 1 Hz yielded an IC_{50} of 5.15 ± 0.5 μM (n_H = 1.2) (Fig. 3 B). Mibefradil also inhibited Nav1.8/SNS currents in a use-dependent fashion, producing full inhibition at 10 μM (0.5 Hz; Fig. 3, C and D). Block of NaN/Nav1.9 and Nav1.8/SNS by mibefradil was reversible within ∼20 min (unpublished data).

Sensitivity of NaN/Nav1.9 Current to the Inorganic Ca^{2+} Channel Blockers

Cadmium. NaN/Nav1.9 currents were isolated by continuous superfusion with 1–3 mM amiloride. As illustrated in Fig. 4 A (a), Cd^{2+} reduced NaN/Nav1.9 currents evoked at a test potential of −60 mV in a dose-dependent manner over the range of 30 to 3,000 μM. It should be noted that currents blocked by Cd^{2+} lacked any hint of the decaying kinetics that characterizes $I_{Ca}T$, as would be expected if some Ca^{2+} currents were left unblocked in the presence of amiloride. We went on to compare Cd^{2+} block of NaN/Nav1.9 current in small neurons to block of $I_{Ca}T$ recorded in D-hair mechanoreceptors, which lacked NaN/Nav1.9 (Fig. 4 A, b) (Fang et al., 2006). The concentration dependence of Cd^{2+} block of normalized currents determined from 11 small DRG neurons and 8 medium-sized D-hair cells conformed to one-to-one dose–response relationships with half-blocking concentrations of 233 ± 5 and 28 ± 2 μM, respectively (Fig. 4 B). Blockade of NaN/Nav1.9 by Cd^{2+} was fully reversible within 5 min. In addition to blocking NaN/Nav1.9 current, Cd^{2+} appeared to shift the I-V curves to more depolarized potentials, without noticeable effect on reversal membrane potential. This trend was more obvious with high concentrations of Cd^{2+} and can be clearly seen when the currents are normalized to

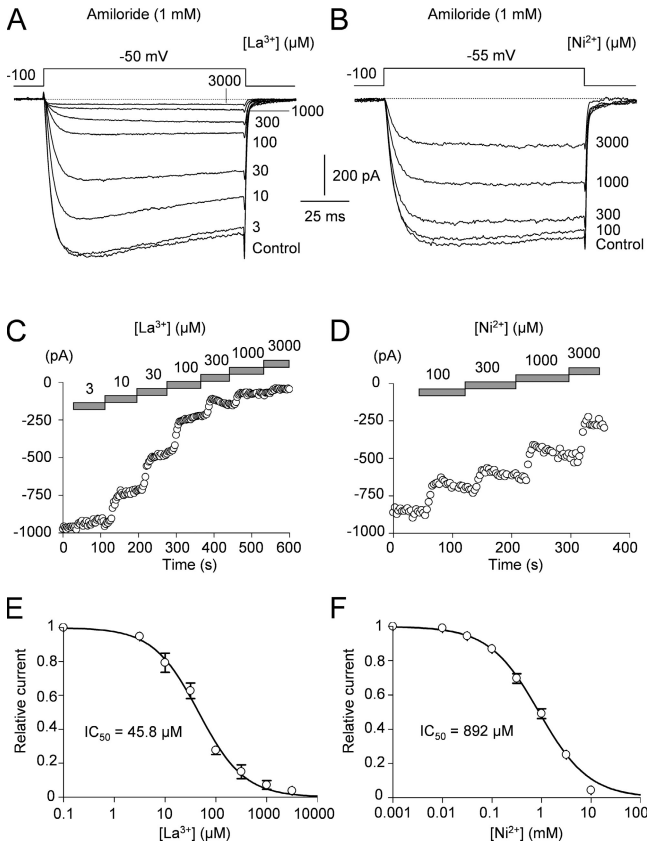

Figure 5. Block of NaN/Nav1.9 in small DRG neurons by lanthanum and nickel. (A and B) Superimposed are NaN/Nav1.9 currents evoked by depolarizing voltage steps to −55 or −50 mV from a holding potential of −100 mV in the presence of increasing concentrations of La^{3+} (3–3,000 μM) (A) or Ni^{2+} (100–3,000 μM) (B). (C and D) Peak NaN/Nav1.9 currents plotted against time in the presence of increasing concentrations of La^{3+} (C) and Ni^{2+} (D). The horizontal bars indicate the time and duration of the drug application. (E and F) Cumulative concentration–inhibition curves for La^{3+} (E) and Ni^{2+} (F). Hill equation was used to fit data points. IC_{50} values were 45.8 ± 3 μM (n_H = 0.96) for La^{3+} and 892 ± 8 μM (n_H = 0.91) for Ni^{2+}. Each data point is the mean ± SEM of 7–12 observations. All experiments were made in the presence of amiloride (1 mM).

the maximum current observed in the absence of Cd^{2+} (Fig. 4 C). Boltzmann curve was shifted 10 mV more positive in the presence of 1,000 μM Cd^{2+} relative to control: ($V_{1/2}$ of −59.5 versus −49 mV, respectively). The degree of block for [Cd^{2+}] above and below the IC_{50} was essentially voltage independent over the potentials tested (Fig. 4 C, top), indicating little intrinsic voltage dependence of Cd^{2+} block. This suggests that Cd^{2+} block of NaN/Nav1.9 resulted from concurrent pore blockade and antagonism of activation, a mechanism reminiscent to that of block of SNS/Nav1.8 current by multivalent cations (Kuo et al., 2004).

Lanthanum and Nickel. La^{3+} and Ni^{2+}, two classical inorganic Ca^{2+} channel blockers, were also tested for ability to block NaN/Nav1.9 current in DRG cells (Fig. 5). Currents recorded in amiloride-containing solution were elicited by stepping to −50 or −55 mV and exposed to increasing concentrations of La^{3+} (Fig. 5 A) or Ni^{2+} (Fig. 5 B), respectively. The time courses of blockade of NaN/Nav1.9 current are also illustrated (Fig. 5, C and D). The dose dependence of La^{3+} and Ni^{2+} blocks did not show major deviation from one-to-one permeation block, with Hill coefficients of 0.96 and 0.91, respectively. The affinities of La^{3+} and Ni^{2+} for NaN/Nav1.9 channels spanned more than one order of magnitude, with La^{3+} being the most effective blocker (IC_{50} = 45.8 ± 3 μM) while Ni^{2+} possesses a 20-fold lower affinity (892.7 ± 8 μM). Although not tested systematically, inhibitions of peak NaN/Nav1.9 current by both cations showed little dependence over the potentials (unpublished data), suggestive that, just like Cd^{2+}, the blocking effects had little intrinsic voltage dependence.

Properties of NaN/Nav1.9 and T-type Ca^{2+} Currents Distinguish Three Subpopulations of Nociceptive Cells

We have devised a classification scheme for the DRG cells we recorded based on the notion that functionally uniform cell populations can be identified by their repertoire of ion channels. Cells were classified according to five cluster variables, namely, cell capacitance (pF) and peak amplitude (normalized for cell size, pA/pF) of NaN/Nav1.9, SNS/Nav1.8, amiloride-sensitive $I_{Ca}T$, and amiloride- and Ni^{2+}-resistant $I_{Ca}T$. We then examined whether each cell cluster was homogeneous with respect to mechanoreactivity and capsaicin sensitivity.

Type-I (C-I) and Type-II (C-II) C-nociceptive Cells. DRG neurons were first assigned to C-nociceptive cells on the basis of their small cell membrane capacitance (14 pF < C_m < 40 pF, n = 78) and the presence of NaN/Nav1.9 current, a marker of nociceptive cells (Benn et al., 2001; Fang et al., 2002). These C-type cells could be readily classified into two distinct, but internally homogeneous, subsets of nociceptive cells with very uniform NaN/Nav1.9 and SNS/Nav1.8 currents but very different $I_{Ca}T$ signatures. Cells clustering in *C-I* type made up 65% of C-nociceptors (C_m = 32 ± 2 pF, range from 25 to 40 pF, n = 51/78) and displayed peak current densities for NaN/Nav1.9 and SNS/Nav1.8 of 12 ± 3 and 36 ± 4 pA/pF, respectively. A representative example of a cell (25 pF) clustered in this subgroup is illustrated in Fig. 6. *C-I* type nociceptive cells exhibited an amiloride-sensitive $I_{Ca}T$, which had a mean peak current density of 6.7 ± 1.1 pA/pF and a half-maximal activation ($V_{1/2}$) of −65 ± 1.5 mV (Fig. 6, A–D). This current was fully blocked by low micromolar concentrations of La^{3+} (10 μM) and Ni^{2+} (50 μM; IC_{50} = 28 μM) (unpublished data). In this category of cells, 1 mM amiloride entirely blocked $I_{Ca}T$, as no LVA currents were left in the presence of low Na^+ (2 mM) external solution (Fig. 6, B and C). NaN/Nav1.9

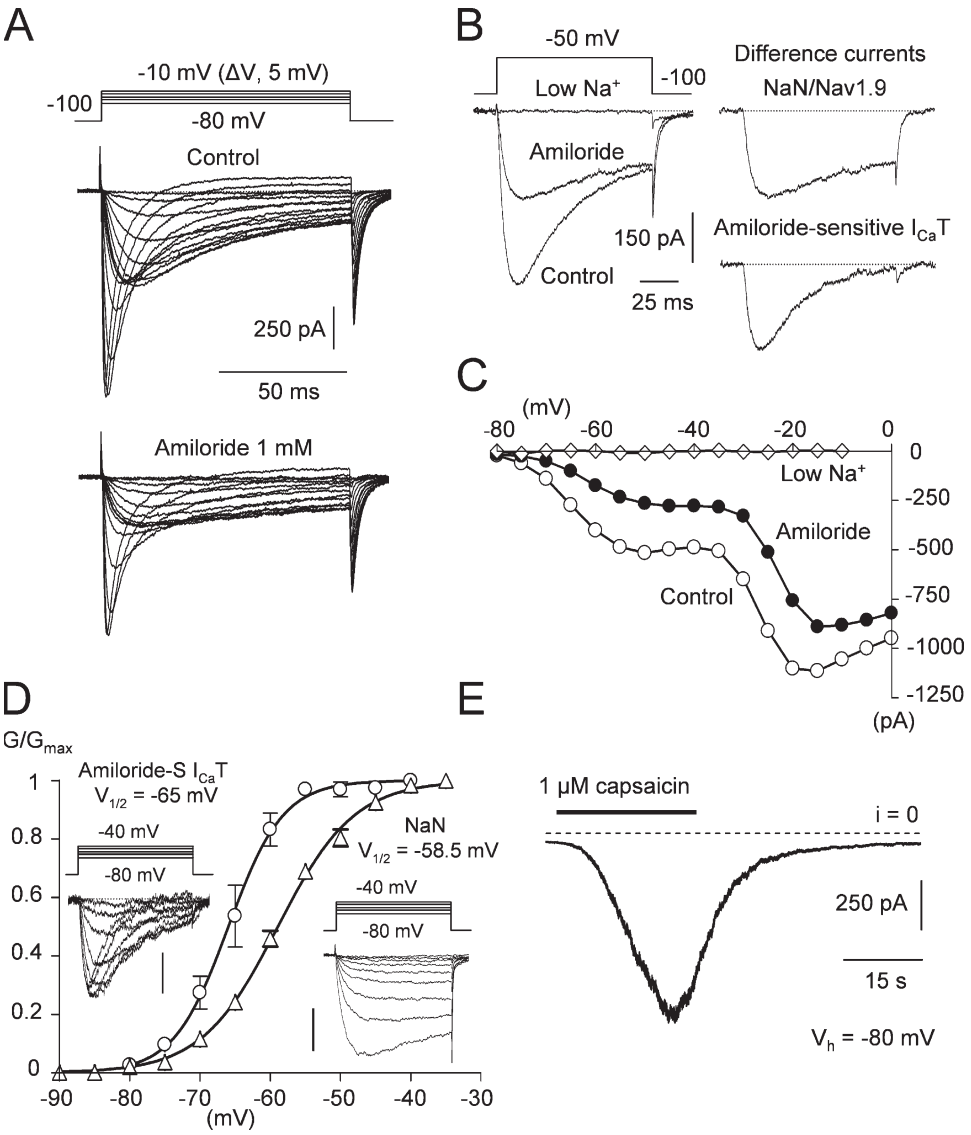

Figure 6. LVA current signature of *C-I* type nociceptive cells. (A–C and E) Same cell. (A) Families of current traces elicited in a small DRG neuron (25 pF) in the absence or presence of 1 mM amiloride. Currents were evoked by 100-ms depolarizations by stepping from −80 to −10 mV in 5-mV increments from a holding potential of −100 mV. Note the marked demarcation between low- and high-threshold currents. Cluster analysis placed 31 small cells into this category. (B) LVA currents evoked at −50 mV in control conditions and after sequential application of amiloride (1 mM) and amiloride-containing low Na^+ solution (2 mM, Low Na^+). The right panels show difference currents, isolating NaN/Nav1.9- and Ca^{2+}-components of the total LVA current. (C) Peak current–voltage relationships for the corresponding neuron illustrated in A, in the absence (Control) or presence of amiloride (1 mM) and after bath application of amiloride-containing low Na^+ solution (Low Na^+). (D) Relative conductances (G/G_{max}) of the amiloride-sensitive $I_{Ca}T$ (○) and NaN/Nav1.9 (△) were plotted against membrane potential and fitted to single Boltzmann functions. The inserts show difference currents isolating the amiloride-sensitive $I_{Ca}T$ and NaN/Nav1.9. Half-activation voltages and slope factors were −65 ± 1.5 and −58.5 ± 1 mV and 4 ± 0.5 and 5.5 ± 0.6 mV, respectively. Note that NaN/Nav1.9 currents were isolated by isoosmotically substituting external Na^+. Bars, 100 pA. Each data point is the mean ± SEM of 11–14 cells. (E) Representative inward current evoked by the application of 1 μM capsaicin at the end of the experiment. 82% of these cells responded to exposure to capsaicin with a mean current of −710 ± 25 pA.

currents characterized in these cells using Na^+ ion substitution had a mean $V_{1/2}$ of –58.5 ± 1 mV (Fig. 6 D). 82% (42/51) of *C-I* type cells responded to capsaicin (1 μM), another marker of nociceptive function (Caterina and Julius, 2001), with a mean inward current of –710 ± 25 pA (Fig. 6 E; pooled data in Fig. 12 A and Fig. 13).

Cells clustering in the second group of C-nociceptive cells (*C-II* type cells) were significantly ($P < 0.05$) smaller (C_m = 21 ± 1.5 pF, range from 14 to 28 pF). They were more rarely encountered and made up 35% of the C-cell population (n = 27/78). Note that these proportions are only indicative since they may vary according to sampling bias and technical limitations (especially when recording small cells). This subset of cells exhibited peak current densities for NaN/Nav1.9 and SNS/Nav1.8 (15.6 ± 4 pA/pF and 37.5 ± 6 pA/pF, respectively) that were not significantly different from those of *C-I* type nociceptive cells, but had a fivefold larger (35.7 ± 8 pA/pF) amiloride-sensitive $I_{Ca}T$ (Figs. 7, A–C). The amiloride-sensitive Ca^{2+} current in these cells had kinetics and voltage dependence essentially identical to *C-I* type nociceptive cells, with a $V_{1/2}$ of −65 ± 0.8 mV and a steepness factor of 4.4 ± 0.3 mV (Fig. 7 F). In addition, these cells also expressed an $I_{Ca}T$ resistant to amiloride (mean peak current density of 5.5 ± 2 pA/pF), as substituting external Na^+ in the presence of amiloride did not abolish LVA currents (Fig. 7 Ab and C–F). The amiloride-resistant $I_{Ca}T$ was fully blocked by 10 μM La^{3+} (Fig. 7, C and E) and, in contrast to the amiloride-sensitive $I_{Ca}T$, was only half-reduced by 260 μM Ni^{2+} (not depicted). This current had inactivation and

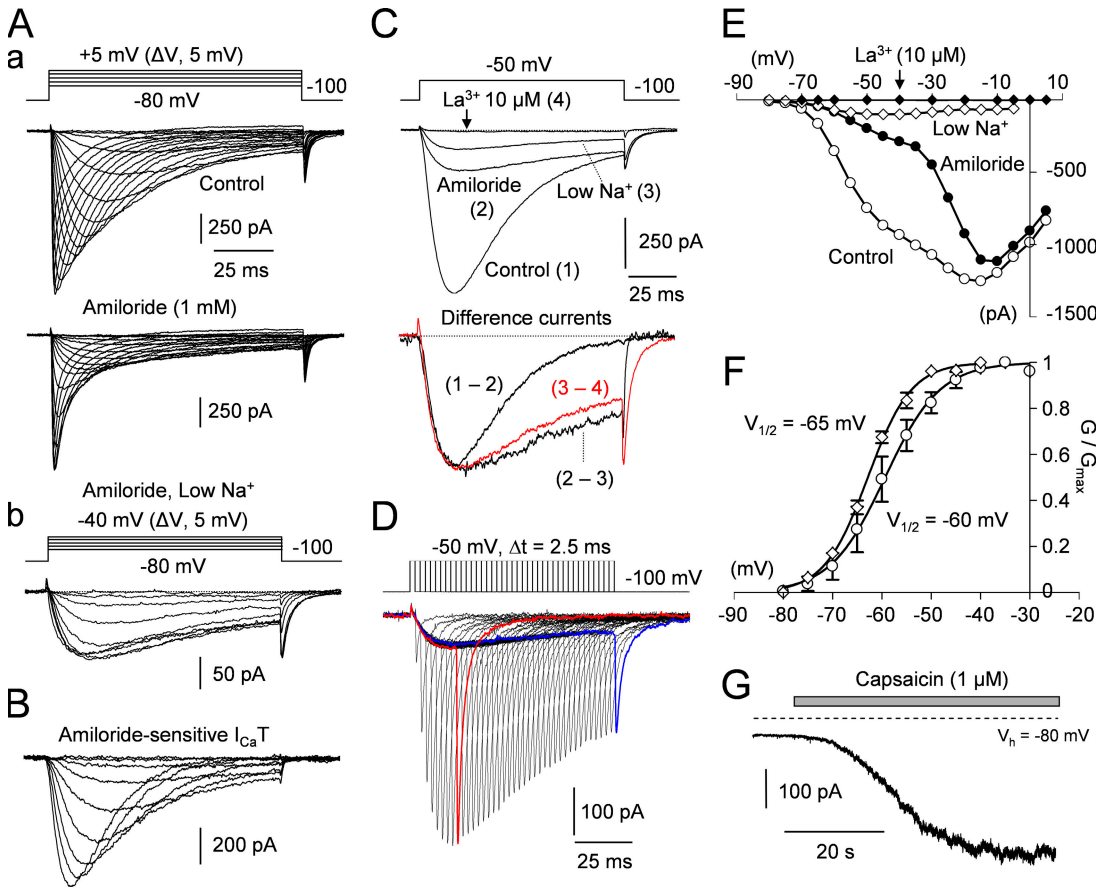

Figure 7. LVA current signature of *C-II* type nociceptive cells. (A–C, E, and G) Same cell. (A) Families of current traces elicited in a small DRG neuron (16 pF) in the absence or presence of 1 mM amiloride (A, a) and in amiloride-containing low Na^+ solution (A, b). Currents were evoked by 100-ms depolarizations as indicated. Cluster analysis placed 27 small cells into this category. (B) Families of amiloride-sensitive $I_{Ca}T$ derived from difference currents in A (a). Voltage protocol as in A (b). (C) Superimposed LVA currents evoked at −50 mV in control conditions (1) and after sequential application of amiloride (1 mM, 2), amiloride-containing low Na^+ solution (Low Na^+, 3), and 10 μM La^{3+} in amiloride-containing low Na^+ solution (4). The bottom panel shows superimposed difference currents determined as indicated, isolating amiloride-sensitive $I_{Ca}T$ (1–2), NaN/Nav1.9 (2–3), and amiloride-resistant $I_{Ca}T$ (3–4, red trace). Note the moderate inactivation and slow tail currents of the amiloride-resistant $I_{Ca}T$. (D) Current traces of the amiloride-resistant $I_{Ca}T$ showing relationships between test pulse duration and tail current amplitude and kinetics. Test pulses were evoked by 2.5-ms depolarization to −50 mV and the pulse duration was lengthened by 2.5 ms between each sweep. Red and blue traces illustrate currents evoked by 22.5- and 100-ms step duration. (E) Peak current–voltage relationships in the absence (Control) or presence of amiloride (1 mM) and after bath application of amiloride-containing low Na^+ solution in the absence (Low Na^+) or presence of La^{3+} (10 μM). (F) The relative conductances (G/G_{max}) of the amiloride-sensitive and amiloride-resistant $I_{Ca}T$ were plotted against membrane potential and fitted to single Boltzmann functions. $V_{1/2}$ and slope factors were −65 ± 0.8 and −60 ± 1.2 mV and 4.4 ± 0.3 and 5.5 ± 0.5 mV, for amiloride-sensitive and amiloride-resistant $I_{Ca}T$, respectively. Each data point is the mean ± SEM of 9–11 cells. (G) Inward current evoked by the application of 1 μM capsaicin at the end of the experiment. 60% of these cells responded to exposure to capsaicin with a mean current of −245 ± 15 pA.

deactivation time constants at −50 and −100 mV, respectively ∼2–3-fold slower than those of the amiloride-sensitive $I_{Ca}T$ (Fig. 7, C and D) and had a $V_{1/2}$ for activation of −60 ± 1.2 mV (Fig. 7 F). 60% of *C-II* type–classified cells responded to capsaicin (1 μM) with relatively small inward currents (−245 ± 15 pA) (Fig. 7 G; pooled data in Fig. 12 A and Fig. 13).

Medium-sized Nociceptive Cells. We identified a third population of cells, which made up ∼32% of the nociceptive cell population (n = 37/115) and which on basis of their C_m (48 ± 3 pF, range 35–70 pF) fell mainly within the medium cell range, possibly corresponding to Aδ-DRG cells. A representative medium-sized nociceptive cell is illustrated in Fig. 8. In this cell, LVA currents were composed of amiloride-sensitive $I_{Ca}T$ and NaN/Nav1.9 current, whereas no amiloride- resistant $I_{Ca}T$ could be detected (Fig. 8, A and B). The predictive validity of this distribution was established by the homogeneity of these currents in these medium-sized cells. In a representative group of 37 neurons, mean peak current amplitudes of NaN/Nav1.9 currents and amiloride-sensitive

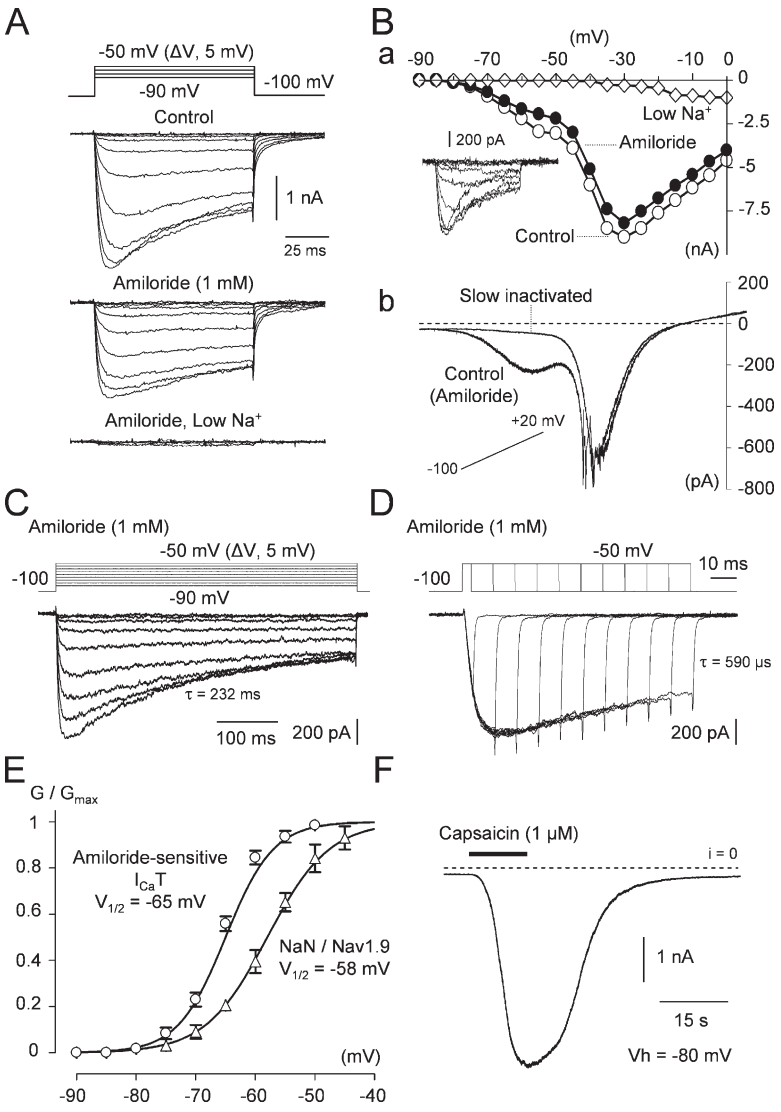

Figure 8. LVA current signature of medium nociceptive cells. (A and B) Same cell. (A) Families of LVA current traces elicited in a medium-sized DRG neuron (42 pF) in the absence or presence of 1 mM amiloride and in amiloride-containing low Na^+ solution. Currents were evoked by 100-ms depolarizations by stepping from −90 to −50 mV in 5-mV increments from a holding potential of −100 mV. Cluster analysis placed 37 medium-sized DRG neurons into this category. (B) Peak current–voltage relationships (B, a) in the absence (Control, ○) or presence of amiloride (1 mM, ●) and after bath application of amiloride-containing low Na^+ solution (Low Na^+, ◇). Inset, families of amiloride-sensitive $I_{Ca}T$ (difference currents). Voltage protocol as in A. (B, b) Superimposed currents elicited by a 10-s ramp depolarization from −100 to +20 mV (rising rate 12 mV s^{-1}) in the presence of amiloride (1 mM) before (control) and after holding the cell at −60 mV for 5 s in order to promote slow inactivation of NaN/Nav1.9 (Slow inactivated). Leak currents were not subtracted in this recording. (C, D, and F) Same cell. (C) Families of NaN/Nav1.9 currents evoked by 500-ms depolarizations in a medium-sized DRG neuron (38 pF) in the presence of amiloride (1 mM). Note the slowly developing inactivation of the NaN/Nav1.9 current at −50 mV (τ = 232 ms; 219 ± 7 ms, n = 12). (D) Superimposed NaN/Nav1.9 currents evoked at −50 mV showing relationships between test pulse duration and tail current amplitude and kinetics. The voltage pulse duration was varied from 4 to 104 ms by 10-ms increments. Note the rapid deactivation time course of NaN/Nav1.9. Time constants obtained from fitting single exponentials to data points are indicated (filtering frequency, 5 kHz). 1 mM amiloride throughout. (E) The relative conductances (G/G_{max}) of NaN/Nav1.9 (△) and amiloride-sensitive $I_{Ca}T$ (○) were plotted against membrane potential and fitted to single Boltzmann functions. $V_{1/2}$ and slope factors were −58 ± 2 and −65 ± 1.2 mV and 5.3 ± 0.2 and 4.1 ± 0.2 mV, for NaN/Nav1.9 and amiloride-sensitive $I_{Ca}T$, respectively. Each data point is the mean ± SEM of 7–10 cells. (F) Inward current evoked by the application of 1 µM capsaicin at the end of the experiment. 75% of these cells responded to exposure to capsaicin with a mean current of −4150 ± 45 pA.

$I_{Ca}T$ were 37.2 ± 7 and 18.5 ± 4 pA/pF, respectively. Within this cell subset, SNS/Nav1.8 amplitudes were typically ≥5 nA (142 ± 20 pA/pF). The lack of amiloride-resistant $I_{Ca}T$ allowed us to precisely investigate the voltage dependence and kinetics of NaN/Nav1.9 current in these cells. Over the whole potential range tested, the inactivation kinetics of NaN/Nav1.9 current is slow (Fig. 8 C) compared with that of the amiloride-sensitive $I_{Ca}T$, with an e-fold change in time constant per 19 and 13.5 mV, respectively (not depicted). The exponential time constant for deactivation of NaN/Nav1.9 observed upon repolarization at –100 mV was 590 ± 5 µs, which is at least twofold faster than that of the amiloride-sensitive $I_{Ca}T$ (1.3 ± 0.1 ms; Fig. 8 D). The amiloride-sensitive $I_{Ca}T$ in Aδ-like nociceptive cells had a $V_{1/2}$ of –65 ± 1 mV, and NaN/Nav1.9 current had a $V_{1/2}$ of –58 ± 2 mV and a steepness factor of 5.3 ± 0.2 mV (Fig. 8 E), which is identical to NaN/Nav1.9 currents expressed in *C-I* and *C-II* type nociceptive cells. Most cells (75%) clustered in these Aδ-like cells had very large capsaicin-induced inward currents (–4150 ± 45 pA) (Fig. 8 F; pooled data in Fig. 12 A and Fig. 13).

High-Threshold Mechanically Activated Cation Currents Distinguish Different Subpopulations of NaN/Nav1.9-expressing Nociceptors

Many nociceptors are polymodal in nature, meaning that they can respond to both mechanical and thermal stimuli (Birder and Perl, 1994). To determine if the neuronal phenotypes we observed correlated with the properties of mechanically activated (MA) currents, cells clustered in *C-I*, *C-II*, and Aδ-like groups were tested for their ability to respond to focal mechanical stimulation. To assess the mechanical sensitivity of a cell,

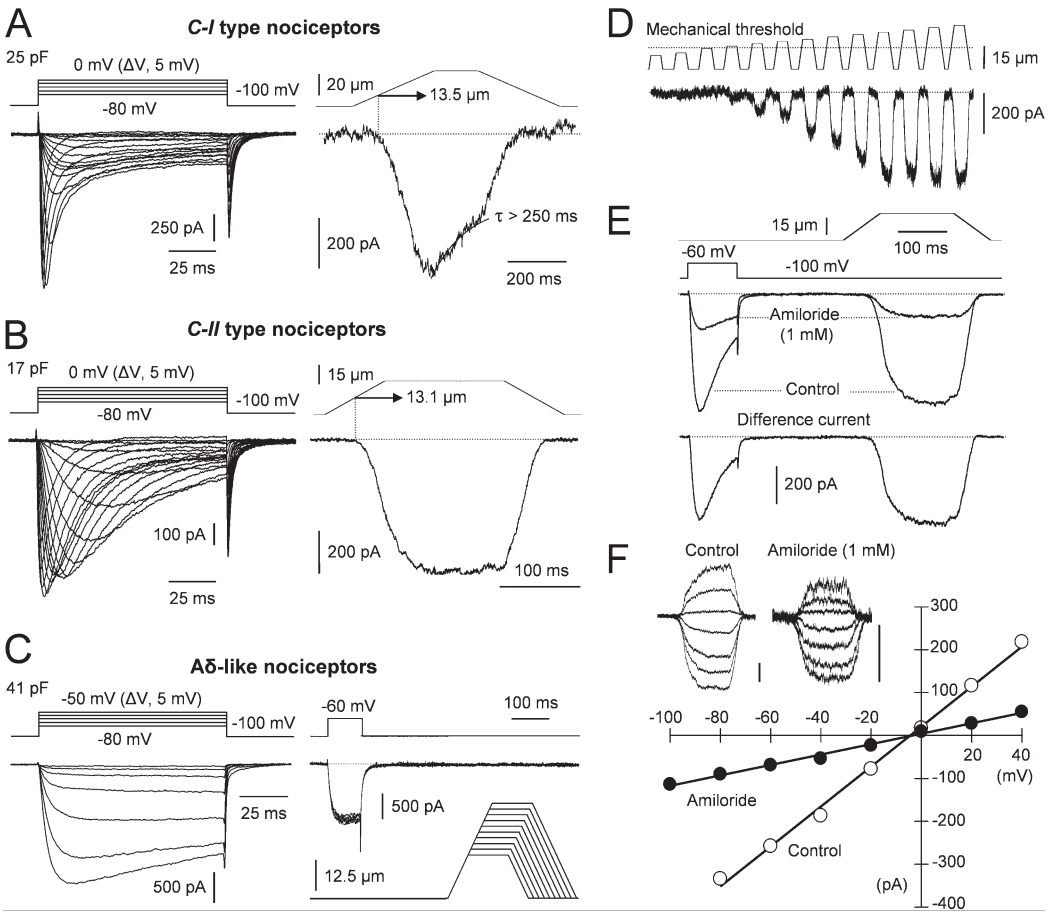

Figure 9. Nociceptors display two types of high-threshold mechanically activated cation currents. (A–C) Representative voltage step–evoked currents and mechanically gated inward currents observed in *C-I* type (25–40 pF, A), *C-II* type (14–28 pF, B) and Aδ-like (35–70 pF, C) nociceptors. Cells were first subjected to 100-ms step depolarizations from a holding potential of −100 mV (as indicated) and then subjected to suprathreshold mechanical stimuli (A and B) or to a series of mechanical steps in 2-µm increments (C). Note that the cell (25 pF) clustering in *C-I* type cells was sensitive to capsaicin (not depicted) and displayed slowly adapting MA currents (A) while the *C-II* type cell (17 pF) was insensitive to capsaicin (not depicted) and had MA currents that failed to adapt during the entire length of the stimulus (B). The minimum distance travelled by the probe to evoke a response in A and B was 13.5 and 13.1 µm, respectively. (C) The cell (41 pF) clustering in the Aδ-like cells was found to be unresponsive to mechanical stimuli. Sweeps were applied at 15-s intervals in C. The velocity of the probe was 200 µm s^{-1} during the ramp segments. (D–F) Same cell as in B. (D) Relationship between pressure strength and the induced mechanical inward current. Sweeps were applied at 15-s intervals but were shown concatenated for clarity's sake. Encoding of the intensity of the stimulus was demonstrated by the graded responses to varying mechanical stimulus applied through the glass probe. Note that amplitude of the MA current saturated as higher pressure was applied. (E) The cell was subjected to dual voltage–mechanical protocol consisting of a 100-ms voltage step from −100 to −60 mV followed by a suprathreshold mechanical stimulus. Amiloride (1 mM) blocked the MA current by ∼80%. (F) Current–voltage relationships of MA current before (○) and after (●) application of 1 mM amiloride. Reversal membrane potential was −5 mV. Inset, cation currents evoked by a 20-µm ramp stimulus at holding potentials ranging from −80 to +40 mV. Bars, 100 pA.

a series of incrementing mechanical stimuli was applied to the cell somata using a small glass probe. This was done before pharmacological tests, as amiloride was found to reduce MA cation currents (see below). Amongst small C-type DRG neurons, we found a clear distinction between MA currents expressed by *C-I* and *C-II* nociceptors (Fig. 9). 20 out of 50 *C-I* nociceptive cells (39%) responded to focal mechanical stimulation of their soma with MA cation currents, of which 15 were found sensitive to capsaicin. MA currents reversed at −3 ± 1 mV (Fig. 9 A). The replacement of Na^+ with other monovalent cations (K^+ and Cs^+) did not shift the reversal potential of MA currents, indicating that mechanosensitive channels do not discriminate these monovalent cations (unpublished data). MA currents turned on during the ramp segment of the command for the forward motion and displayed slowly adapting kinetics with time constants ranging from 200 to 400 ms (Fig. 9 A, right). Such MA currents peaked concurrently with cessation of the probe movement and declined when pressure had been released. The minimum distance travelled by the probe to evoke a response in these cells was 13 ± 2 µm, which was approximately two times higher than pressures for mechanical activation of

low-threshold mechanoreceptors (see below). Therefore, because of their relatively high pressure threshold and sensitivity to capsaicin, most *C-I* nociceptors were tentatively classified as high-threshold C-mechanoheat (possibly polymodal) nociceptors. High-threshold MA currents in these cells were inhibited by 79 ± 6% by 1 mM amiloride, irrespective of the capsaicin sensitivity of the cell (unpublished data; see Fig. 12 C).

Although *C-II* type nociceptors had somewhat smaller cell bodies, which rendered difficult systematic investigation of their mechanical sensitivity, MA currents could be evoked in 32% of these cells (Figs. 9, B and D–F), of which very few (1/9) were found to be responsive to capsaicin. These MA currents were activated by relatively high pressure (14 ± 2 μm; Fig. 9 B). Therefore, mechanoreactive *C-II* cells were tentatively classified as high-threshold C-mechanonociceptors. MA currents had reversal potential of −4 ± 2 mV and nearly linear *I-V* relationships in asymmetrical solution, indicating nonselective permeability. In contrast to *C-I* nociceptors, MA currents in *C-II* nociceptive cells did not decline in amplitude during the stationary part of the 200-ms stimulus, i.e., showed nonadapting kinetics (Fig. 9 B). Kinetics analysis further revealed an interesting additional facet of these nonadapting MA currents. Typically, current amplitude continued to increase for a period of 10–30 ms after the cessation of probe movement, whereas the current declined as soon as the pressure was removed. In addition, the amplitude of repeatedly evoked nonadapting MA currents could be stable for up to 2 h and typically reached a plateau as higher pressures were applied (Fig. 9 D). Nonadapting MA currents were inhibited by 82 ± 3% by 1 mM amiloride (Fig. 9 E and Fig. 12 C). No MA whole-cell currents could be evoked in Aδ-like nociceptive cells using the most intense mechanical stimuli that could be applied to the neuron without disrupting the seal (Fig. 9 C).

D-hair Cells Express Low-threshold, Rapidly Adapting MA Cation Currents, and Different T-type Ca^{2+} Currents

Cells that were classified as D-hair cells had medium-diameter cell bodies (54 ± 5.6 pF, range 39–65 pF). They proved to be substantially different from other current signature-classified cells in that they displayed very typical $I_{Ca}T$ ("giant $I_{Ca}T$"; Shin et al., 2003; Dubreuil et al., 2004) and were insensitive to capsaicin (1 μM). All the cells clustered in this subgroup exhibited uniform MA cation currents (E_{rev} ∼−2 mV), which typically required low stimulus intensity to activate (Fig. 10 A). The minimum distance travelled by the probe to evoke a response was 6.5 ± 1.5 μm, thereby classifying these cells as low-threshold mechanoreceptors. MA currents in D-hair cells had rapidly adapting kinetics with time constants ranging from 10 to 50 ms. Encoding of the intensity of the stimulus was demonstrated by the graded responses to varying mechanical stimulus applied through the glass probe. It should be noted that suprathreshold mechanical stimuli typically evoked MA currents with both transient and sustained components (Fig. 10 A, inset). Low-threshold MA cation currents in D-hair cells were found to be more sensitive to amiloride than high-threshold MA currents in C nociceptive cells, with 95 ± 3% block by 1 mM amiloride (Fig. 10 B and Fig. 12 C).

LVA inward currents in D-hair mechanoreceptive cells did not appear to be fully antagonized by 1–3 mM amiloride (Fig. 10, C and D). Substituting external Na^+ revealed that D-hair cells also displayed an amiloride-resistant $I_{Ca}T$. This current was fully blocked by 10 μM La^{3+} but showed little sensitivity to Ni^{2+} (IC_{50} = 245 μM; unpublished data). Fig. 10 (C–E) illustrates the two components of $I_{Ca}T$ in a single D-hair cell (52 pF). In a representative group of 39 cells, mean peak amplitudes of the amiloride-sensitive and amiloride-resistant $I_{Ca}T$ were 93.3 ± 26 and 10.9 ± 3 pA/pF, respectively. Their voltage dependence ($V_{1/2}$ of −65 ± 1.5 and −63 ± 1.5 mV, respectively) was not significantly different from those in *C-II* nociceptors (Fig. 10 E). Note that a small Nav1.8/SNS-like current (11.9 ± 4 pA/pF, n = 18), but not Nav1.9/NaN, was routinely detected in D-hair mechanoreceptive cells (arrow in Fig. 10 D, Fig. 12 A, and Fig. 13).

Large (Aα/β-like) DRG Cells Express Low-Threshold, Intermediately Adapting MA Cation Currents, Different T-type Ca^{2+} Currents, but No LVA TTX-R Na^+ Currents

Cells that clustered in this subgroup fell within the large cell range (70–105 pF) and in all cases but one were found to be insensitive to capsaicin. In addition to difference in size, these cells displayed distinguishing current signatures that serve to discriminate them from other cell types. (a) LVA currents were conducted essentially through amiloride-sensitive and amiloride-resistant $I_{Ca}T$, while LVA TTX-R Na^+ currents were undetectable (Fig. 11, A and B). In a representative group of 18 cells, mean peak amplitudes of the amiloride-sensitive and amiloride-resistant $I_{Ca}T$ were 10 ± 3 and 3.75 ± 2.5 pA/pF, respectively. (b) These cells had powerful HVA I_{Ca}, which was two- to threefold larger in amplitude than those in D-hair cells (comparison using CsCl-based pipette solution; see Materials and methods). (c) Relatively small SNS/Nav1.8-type currents were seen in these large cells with a mean peak current amplitude of 12.5 ± 5 pA/pF. (d) All these cells exhibited MA cation currents (E_{rev} = −3 ± 1 mV), which had intermediately adapting kinetics with voltage-independent time constants ranging from 70 to 90 ms (Fig. 11, C and D). These MA currents activated in response to small probe displacements (8 ± 1 μm) and were equally permeable to K^+, Na^+, and Cs^+ and less to Ca^{2+} with a P_{Ca}/P_{Na} selectivity of 1–3. In contrast to other cell types, MA cation currents in large cells were less susceptible to block by

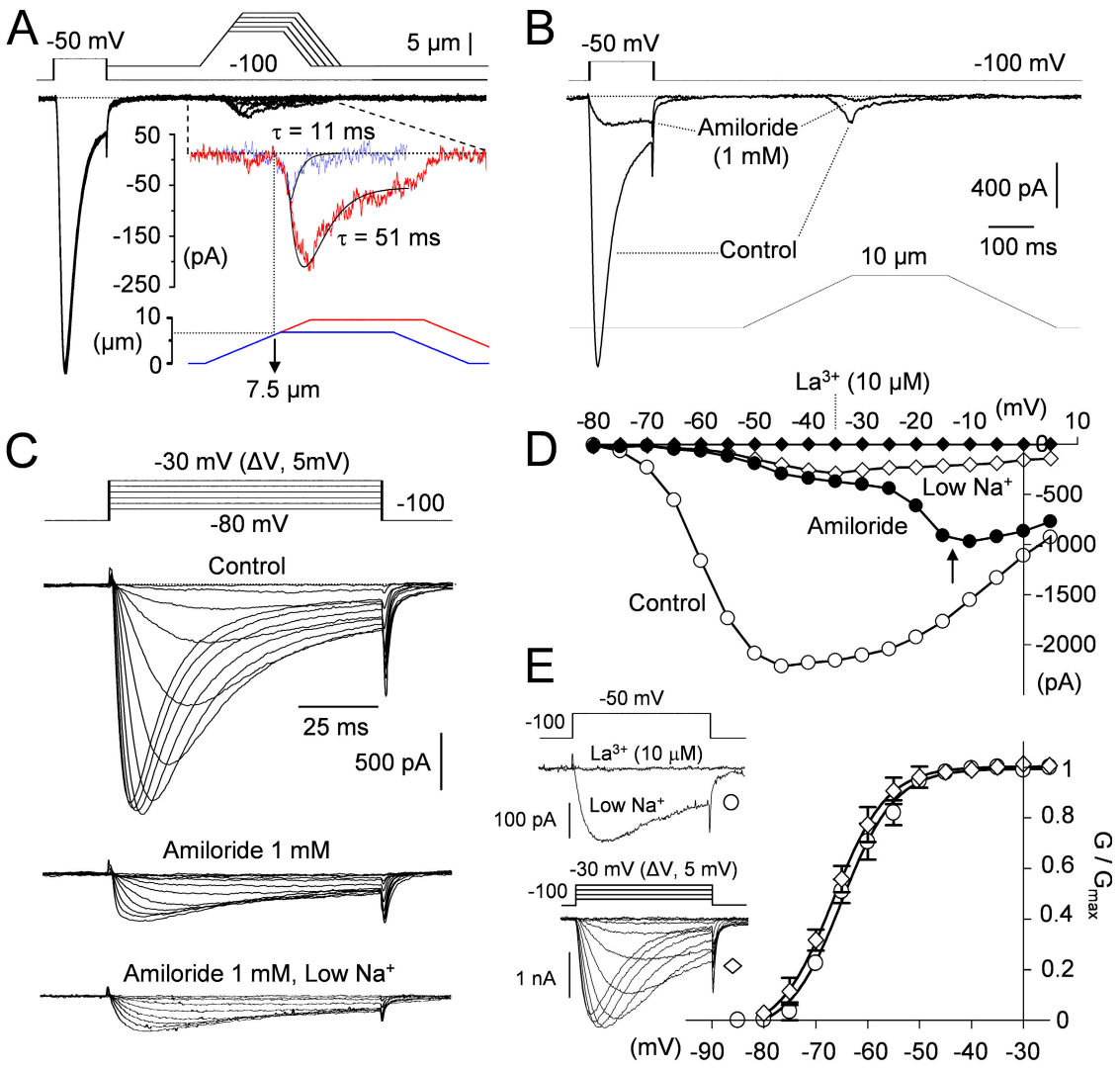

Figure 10. Medium-sized D-hair cells express low-threshold, rapidly adapting MA currents and two pharmacologically distinct $I_{Ca}T$. (A–D) Same cell. (A) A medium-sized D-hair cell (52 pF) was subjected to dual voltage–mechanical protocol consisting of a 100-ms voltage step from −100 to −50 mV followed by a series of incrementing (1 µm) mechanical stimuli. Sweeps were applied at 15-s intervals to allow MA currents to recover fully. D-hair cells are identifiable by the presence of large $I_{Ca}T$. The minimum distance travelled by the probe to evoke a response was 7.5 µm, thus this cell was classified as low-threshold mechanoreceptor. Note that at mechanical threshold, a transient, rapidly adapting inward current was evoked while suprathreshold stimuli evoked a current with both transient and sustained components. The velocity of the probe was 200 µm s^{-1} during the ramp segments. (B) Both $I_{Ca}T$ and MA currents were inhibited by amiloride (1 mM). (C) Families of LVA currents evoked in the D-hair cell by 100-ms depolarizations from −80 to −30 mV in 5-mV increments in control, in the presence of amiloride (1 mM) and after bath application of amiloride-containing low Na^+ solution. (D) Peak I-V relationships in the absence (Control, ○) or presence of amiloride (1 mM, ●) and after bath application of amiloride-containing low Na^+ solution in the absence (Low Na^+, ◇) or presence of La^{3+} (10 µM, ◆). Note that in this cell, as in most D-hair cells, a small SNS/Nav1.8-like current is seen (indicated by the arrow; see also Fig. 13). (E) The relative conductances (G/G_{max}) of the amiloride-sensitive (◇) and amiloride-resistant (○) $I_{Ca}T$ were plotted against membrane potential and fitted to Boltzmann functions. $V_{1/2}$ and slope factors were −65 ± 1.5 and −63 ± 1.5 mV and 4.7 ± 0.2 and 5 ± 0.1 mV, respectively. Each data point is the mean ± SEM of 7–14 cells. Insets, amplitude of the amiloride-resistant $I_{Ca}T$ was estimated as the La^{3+}-sensitive component of LVA currents determined in the amiloride-containing low Na^+ solution, whereas the amiloride-sensitive $I_{Ca}T$ is obtained by difference currents derived from experiments as in C. This type of cells was found to be unresponsive to capsaicin.

amiloride with 45 ± 4% inhibition by 1 mM amiloride (Fig. 11 E and Fig. 12 C). Most notably, only the adapting component but not the sustained component of the MA cation current was suppressed by amiloride in this cell subset (Fig. 11 E).

DISCUSSION

Using pharmacological discriminating tools we have broken down LVA currents in single DRG neurons and provided a thorough description of the specific contribution of Ca^{2+} and Na^+ current complements into five

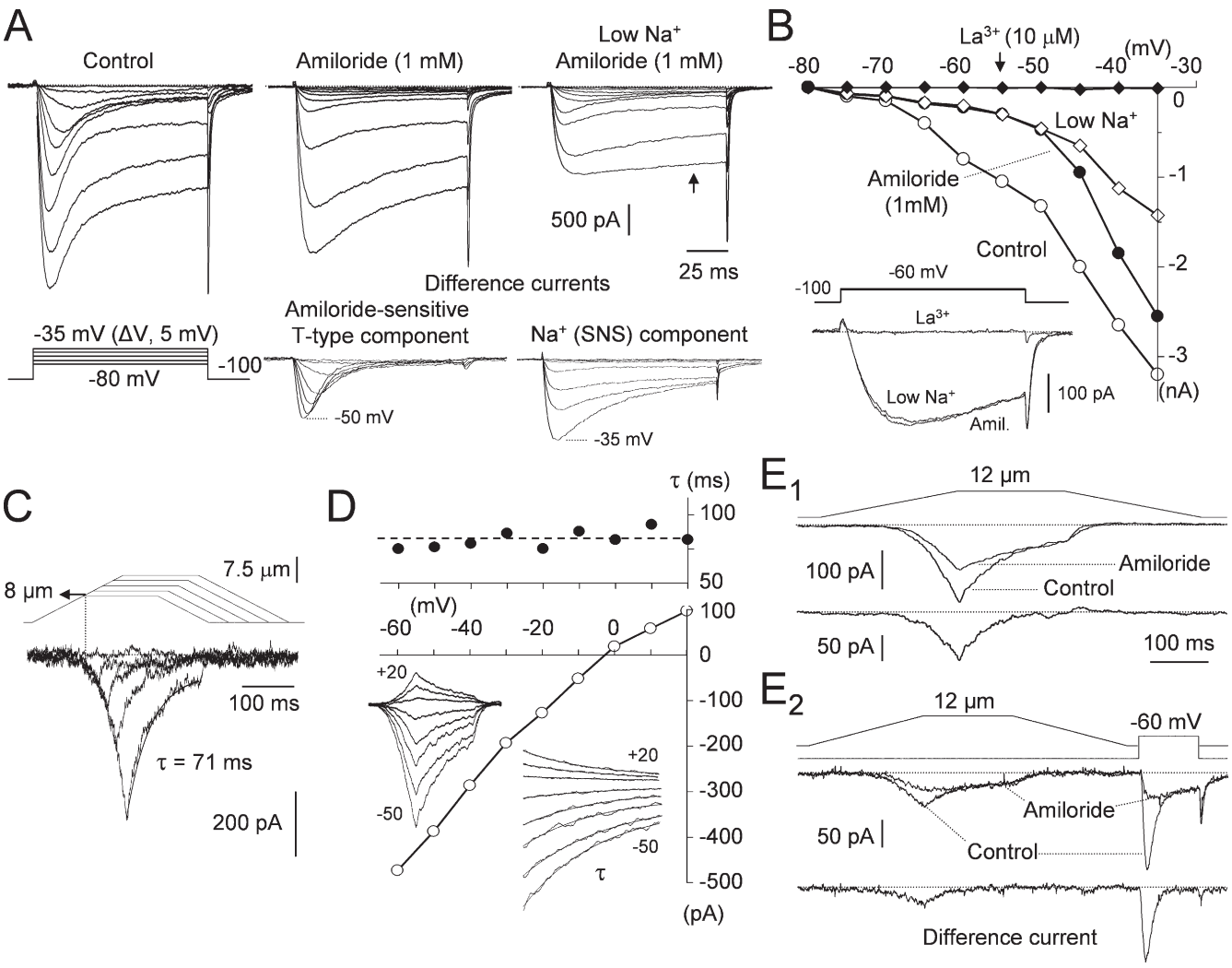

Figure 11. Large-diameter DRG cells lacking NaN/Nav1.9 express low-threshold intermediately adapting MA currents and two types of $I_{Ca}T$. (A–E) Same cell. (A) Families of current traces elicited in a large DRG neuron (87 pF) in the absence (Control) or presence of 1 mM amiloride and in amiloride-containing low Na^+ solution. Currents were evoked by 100-ms depolarizations by stepping from −80 to −35 mV in 5-mV increments from a holding potential of −100 mV. Cluster analysis placed 18 large-sized DRG neurons into this category. Bottom traces show difference currents isolating the amiloride-sensitive $I_{Ca}T$ (steps from −80 to −50 mV) and the TTX-R SNS-like current (steps from −80 to −35 mV). Note that in addition to amiloride-resistant $I_{Ca}T$, these large cells also expressed large high-threshold I_{Ca} (arrow), which was partially blocked by our fluoride-containing pipette solution. (B) Peak I-V relationships in the absence (Control, ○) or presence of amiloride (1 mM, ●) and after bath application of amiloride-containing low Na^+ solution in the absence (◇) or presence of La^{3+} (10 μM, ◆). Inset, block of the amiloride-resistant $I_{Ca}T$ by 10 μM La^{3+} in the presence of low Na^+ external solution. (C) MA currents evoked by a series of incrementing (1.5 μm) mechanical stimuli at a holding potential of −80 mV. The minimum distance travelled by the probe to evoke a response was ∼8 μm, thus this cell was classified as low-threshold mechanoreceptor. Note that decay kinetics of MA currents had time constants in between slowly adapting nociceptors and rapidly adapting D-hair cells. Sweeps were applied at 15-s intervals; probe velocity, 200 μm s^{-1}. (D) Amplitude (bottom, ○) and decay kinetics (top, ●) of the MA current plotted as a function of holding potential. The cell was held at V_h for at least 20 s before the mechanical stimulation (15 μm) was applied. The holding currents were subtracted for clarity. Inset, MA currents evoked by a 15-μm ramp stimulus at holding potentials ranging from −50 to +20 mV. The expanded time scale shows monoexponential fits to the current decay. (E_1) Normal external solution. (E_2) Low Na^+ external solution ($[Ca^{2+}]_o$ = 2.5 mM). The cell was subjected to a suprathreshold mechanical stimulus (E_1) or dual mechanical–voltage protocol (E_2) consisting of a suprathreshold mechanical stimulus followed by a 100-ms voltage step to −60 mV. Note that under both conditions, amiloride (1 mM) suppressed the rapidly adapting component of the low-threshold MA current but not the more sustained component. This cell was found to be unresponsive to capsaicin.

main, electrophysiologically uniform groups of DRG neurons (Figs. 12 and 13). These subspecialized groups of DRG neurons are also distinguished by the specific expression of mechanical cation currents, which had different biophysical properties. Our results therefore provide insights into how electrogenesis and sensory modalities are specified in different populations of DRG receptors.

Pharmacological Dissection of NaN/Nav1.9 Current and T-type Ca^{2+} Currents in DRG Cells

A major purpose of this paper was to present a view of DRG cell LVA channel heterogeneity developed from over 3 years work on DRG neurons. We first sought to identify the different components of LVA currents in single cells by defining a method for better separation of NaN/Nav1.9 and $I_{Ca}T$. One major finding is that amiloride, but not inorganic Ca^{2+} channel blockers, can be readily used to discriminate $I_{Ca}T$ and NaN/Nav1.9 current. Using amiloride as a discriminative agent, we provided evidence that LVA currents measured in each of the 338 cells included in this study were composed of NaN/Nav1.9 and/or amiloride-sensitive $I_{Ca}T$, which coexisted with various extents from one cell to the other. Moreover, it quickly became apparent that under conditions where NaN/Nav1.9 was eliminated, total $I_{Ca}T$ was not fully inhibited by amiloride. The amiloride-resistant $I_{Ca}T$, which has been overlooked in previous studies, could be unambiguously distinguished from amiloride-sensitive $I_{Ca}T$ on both pharmacological and biophysical grounds. In addition to differences in amiloride sensitivity, this current was also distinct in its sensitivity to Ni^{2+}, with an IC_{50} of 240–260 μM, which is ~10-fold higher than that of the amiloride-sensitive $I_{Ca}T$ (28 μM). Recorded under physiological $[Ca^{2+}]_o$, the two identified types of $I_{Ca}T$ have very similar voltage dependence, with amiloride-sensitive $I_{Ca}T$ activating at most negative and amiloride-resistant $I_{Ca}T$ at slightly more positive potentials.

Three types of $I_{Ca}T$, Cav3.1, Cav3.2, and Cav3.3, have been cloned (Cribbs et al., 1998; Perez-Reyes et al., 1998; Lee et al., 1999). Based on kinetics data and the fact that of the three cloned T-channels only Cav3.2 is blocked by micromolar concentrations of Ni^{2+} while much higher concentrations are required to half-block Cav3.1 (250 μM) and Cav3.3 (216 μM) (Lee et al., 1999; Perez-Reyes, 2003), we suggest that the Cav3.2 channel profile corresponds closely to that of the amiloride-sensitive $I_{Ca}T$. On the other hand, the slow inactivation kinetics of the amiloride-resistant $I_{Ca}T$, along with its relative resistance to Ni^{2+} and amiloride, may support the assumption that Cav3.3, which gives rise to slowly inactivating $I_{Ca}T$ (Gomora et al., 2002), represents the counterpart of the amiloride-resistant $I_{Ca}T$. This is in accord with in situ hybridization data, which showed that DRG cells express Cav3.2 and Cav3.3 mRNA but no Cav3.1 mRNA (Talley et al., 1999). This inference is supported by the observations that peripheral pain behavior is unaffected in Cav3.1$^{-/-}$ mice (Kim et al., 2001) and that expression level of the Cav3.3 gene is reduced in NT-4$^{-/-}$ mice, indicating that Cav3.3 is co-expressed with Cav3.2 in D-hair mechanoreceptors (Shin et al., 2003).

A logical extension of these findings was to determine the pharmacological profile of NaN/Nav1.9, which was still largely unknown. Particular attention has been directed toward defining complete concentration–response curves for Ca^{2+} channel blockers in order to allow detailed comparison with similar data from other channels. Several important findings have come from

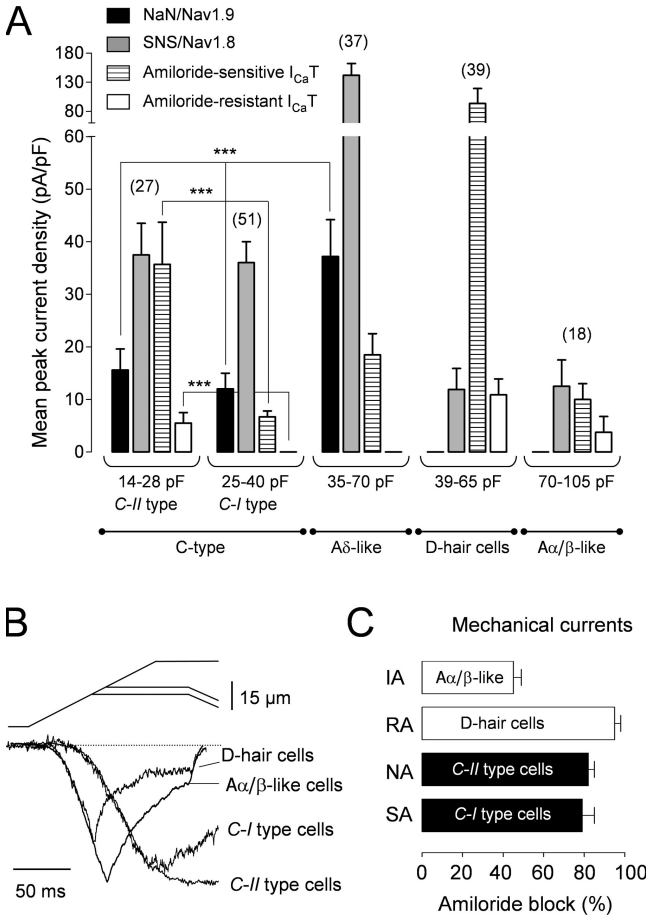

Figure 12. Distribution patterns of ion currents in subclassified sensory neurons. (A) Histogram illustrating current signatures of small, medium, and large DRG neurons. Cells were classified according to their size and to the pattern of NaN/Nav1.9, SNS/Nav1.8, amiloride-sensitive and amiloride-resistant $I_{Ca}T$. Based on these variables, cluster analysis identified five main populations among the 162 DRG cells that could be successfully tested for the entire battery of characteristics. 82, 60, 75, 0, and 5.5% of *C-I* type, *C-II* type, Aδ-like, D-hair, and Aα/β-like cells were sensitive to capsaicin. Note that whether cells were sensitive to capsaicin or not, all cells clustering as *C-I* type, *C-II* type, and Aδ-like cells had uniform LVA current signatures. Bars represent the mean ± SEM and numbers in the parentheses denote the number of cells for each class. ***, $P < 0.005$. (B) Comparison between representative MA currents evoked by mechanical ramp stimuli in D-hair cells, Aα/β-like cells, and *C-I* and *C-II* type nociceptors. Note the difference in threshold and kinetics of MA currents in these four subclassified cell classes. Time constants of adapting kinetics of MA currents in *C-I* nociceptors, D-hair cells, and Aα/β-like cells were significantly different ($P < 0.05$; one-way ANOVA) and were 275 ± 14 ms, 42 ± 5 ms, and 79 ± 6 ms, respectively. (C) Inhibition (mean ± SD) of peak MA currents by 1 mM amiloride. RA, rapidly adapting; IA, intermediately adapting; SA, slowly adapting; NA, nonadapting.

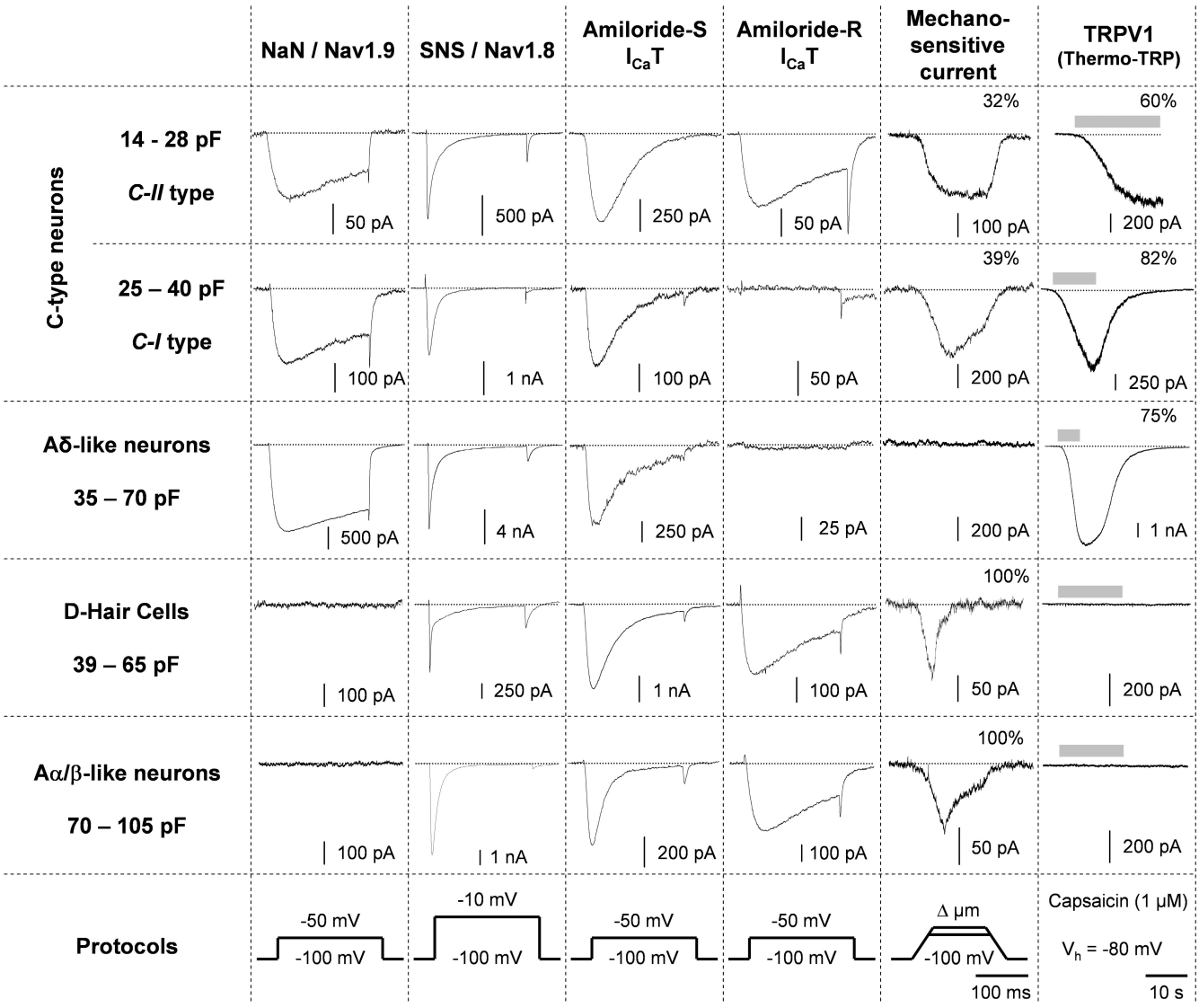

Figure 13. Current signatures of nociceptors and mechanoreceptors. Current signature patterns evoked by voltage steps (100 ms), mechanical stimulation, and drug application are shown for each cell population. The protocol waveforms are illustrated in the bottom row. Five distinct cell types were identified from small-, medium-, and large-diameter cell populations. *C-I* and *C-II* type nociceptors are distinguished by the amplitude of the amiloride-sensitive $I_{Ca}T$ (Cav3.2), the presence of amiloride-resistant $I_{Ca}T$ (putative Cav3.3), and, when detected, the properties of the MA current. The combination of large amiloride-sensitive $I_{Ca}T$ (Cav3.2), rapidly adapting MA currents, unresponsiveness to capsaicin, and absence of NaN/Nav1.9 is particularly important to distinguish D-hair cells from medium-sized Aδ-like cells. The low-threshold mechanoreceptors, Aα/β-like and D-hair cells, are distinguished by the kinetics of their MA currents. The approximate incidence (%) is indicated when necessary.

the present investigations. First, inorganic Ca^{2+} channel blockers are potent inhibitors of NaN/Nav1.9, with the following rank order (IC_{50}): La^{3+} (46 µM) > Cd^{2+} (233 µM) > Ni^{2+} (892 µM). Metal cations had two effects: they blocked NaN/Nav1.9 and shifted the voltage dependence of gating, suggestive of two sites of action. This dual mechanism via pore block and antagonistic effect on channel activation has previously been reported for block of SNS/Nav1.8 (Kuo et al., 2004). Thus, our data indicate that NaN/Nav1.9 shares pharmacological properties with $I_{Ca}T$, raising some doubt as to the suitability of metal cations as agents capable of distinguishing NaN/Nav1.9 from Ca^{2+} channels. Moreover because Cd^{2+} can alter NaN/Nav1.9 gating, our results emphasize that absence of multivalent cations is critical in assaying functional properties of NaN/Nav1.9 channels. By doing so with the use of amiloride, we demonstrated that NaN/Nav1.9 current was selectively, although variably, expressed in *C-I*-, *C-II*-, and Aδ-nociceptive cells, in agreement with immunological studies (Fang et al., 2002). Second, we show that mibefradil, a preferential $I_{Ca}T$ antagonist, is a potent blocker of NaN/Nav1.9 (IC_{50}, 5 µM). Mibefradil blocked NaN/Nav1.9 in a frequency-dependent manner, indicating preferential binding to

states visited during the depolarization. Moreover, the degree of block correlated well with the extent of the slow inactivation (unpublished data), suggesting that the slow time course of block during repeated stimulation results from interaction with slow-inactivated NaN/Nav1.9 channels. State-dependent block by mibefradil has been recently shown for other Na^+ channel isoforms, including the TTX-R Nav1.5 (McNulty and Hanck, 2004). Thus, although mibefradil exhibits a higher affinity in blocking $I_{Ca}T$ over HVA Ca^{2+} currents (Clozel et al., 1997; Martin et al., 2000), it also has micromolar affinity for NaN/Nav1.9 channels, pointing to a potentially common mibefradil-binding motif across targets. Given that mibefradil is known to reverse some experimental pain states (Todorovic et al., 2002; Dogrul et al., 2003), such cross-reactivity with NaN/Nav1.9, another important target for antinociceptive agents, suggests that mibefradil's antinociceptive actions might involve interaction with multiple ion channels rather than selective inhibition of $I_{Ca}T$.

Electrophysiologically Defined DRG Cells Express Distinct Mechanosensitive Channels

Based on ion channel signatures, five groups of internally homogeneous DRG cells could be distinguished by cluster analysis (see Fig. 12 A and Fig. 13). Small DRG cells could be subdivided into two groups that represented 65% (*C-I* type) and 35% (*C-II* type) of C-cells. Systematic delineation of *C-I* and *C-II* type cells showed that they display identical densities of NaN/Nav1.9 and Nav1.8/SNS currents. Despite these similarities, clustered *C-II* cells could be readily distinguished from *C-I* type cells by an approximately fivefold larger $I_{Ca}T$. We showed that $I_{Ca}T$ arises from both Cav3.2 and possibly Cav3.3 channels, with a prominent contribution of the former. These cells closely resemble a novel class of small DRG cells recently designated as "T-rich" and which have prevalent T-type over HVA Ca^{2+} currents (Nelson et al., 2005). Although it is difficult to place our cell classes in direct comparison with previous studies due to different strategies of characterizing cells, our *C-I* type cells match the type-1 cells of Cardenas et al. (1995) and Petruska et al. (2000) with respect to cell size, capsaicin-currents, and $I_{Ca}T$ density. Based on capsaicin sensitivity and mechanoreactivity, we propose that *C-I* type cells comprise C-thermonociceptors and C-mechanoheat nociceptors, while *C-II* type cells contain two subspecialized groups principally composed of C-thermonociceptors and C-mechanonociceptors.

During the course of recordings, we also examined the signatures of 96 medium cells, from which 66 could be studied in detail and fell into two uniform classes (Fig. 12 A and Fig. 13). Cells tentatively classified as Aδ-nociceptors are mostly responsive to capsaicin and have large NaN/Nav1.9 and substantial Cav3.2 current but no sizeable amiloride-resistant $I_{Ca}T$, whereas D-hair cells, besides being insensitive to capsaicin and lacking NaN/Nav1.9, can be reliably identified by their "giant" Cav3.2 current (White et al., 1989; Cardenas et al., 1995; Shin et al., 2003; Dubreuil et al., 2004) (Fig. 12 A and Fig. 13). Cells clustering in the fifth group, possibly corresponding to Aα/β-mechanoreceptors, were generally capsaicin insensitive, had small $I_{Ca}T$, had no NaN/Nav1.9 current, and exhibited powerful HVA Ca^{2+} currents in agreement with Scroggs and Fox (1992). In addition, it should be noted that SNS/Nav1.8 current was found to be prominently expressed in cells classified as nociceptive (Fig. 12 C and Fig. 13), which correlates well with the notion that broad somatic action potential is a fingerprint of nociceptive units in vivo (Fang et al., 2005).

Current signature-identified cells were uniform in term of mechanosensitivity. Mechanoreactive cells in *C-I* and *C-II* groups responded primarily to the static phase of the stimulus and to high levels of mechanical force, suggestive of their putative function as high-threshold mechanonociceptors. Importantly, the observation that MA currents in *C-I* and *C-II* cells have distinct inactivation rates (Fig. 12 B) suggests that they may differentially shape the electroresponsiveness of receptor endings. In this regard, it is important to note that the kinetics of MA currents in *C-I* (slowly adapting) and *C-II* (nonadapting) nociceptive cells in the present study are well suited to sustain the discharges observed in vivo in C-mechanoheat nociceptors (e.g., slowly adapting) and C-mechanonociceptors (e.g., ∼sustained), respectively (see Fig. 2 in Lewin and Moshourad, 2004).

In contrast, medium and large nonnociceptive DRG cells responded to the ramp phase of the stimulus and to low levels of mechanical force, with either rapidly (D-hair cells) or intermediately (Aα/β-like cells) adapting MA currents, consistent with their function as low-threshold mechanoreceptors. These MA currents are also well suited to sustain the in vivo activity of rapidly adapting D-hair mechanoreceptors and "slowly" adapting Aα/β-mechanoreceptors, respectively (see Lewin and Moshourab, 2004).

Unexpectedly, Aδ-neurons were refractory to mechanical stimulation. Given the common polymodal nature of these cells (Lawson, 2002), it is possible that Aδ-like cells have higher mechanical thresholds that were not reached before disruption of pipette seals. Of relevance, TRPA1, which has just been suggested to contribute to mechanotransduction in C-fiber nociceptors (Kwan et al., 2006; but see Bautista et al., 2006), is not expressed in Aδ mechanonociceptors (Kobayashi et al., 2005). Therefore it is likely that another high-threshold MA channel exists in Aδ mechanonociceptors.

Nonselective currents activated by pressure applied to the soma were previously reported in DRG neurons (McCarter et al., 1999; Drew et al., 2002, 2004). These currents were generally consistent with the MA currents

observed in the present study. We have however obtained contradictory results concerning the pharmacology of the MA currents in that we found that MA currents in different DRG cell subpopulations are inhibited by amiloride, though with various extent (Fig. 12 C). This is at odds with data by Drew et al. (2002), which showed no effects of amiloride on MA currents but accords well with those by McCarter et al. (1999), which reported that MA currents in DRG cells are sensitive to the amiloride derivative benzamil. Nevertheless, the diversity of mechanosensitive channel kinetics, threshold, and pharmacological sensitivity means that different types of channels, although possibly related, are involved in the transduction processes of low- and high-threshold mechanoreceptors. Furthermore, our study also provides some hints that the high-threshold mechanotransducer in nociceptive neurons may not be a single channel entity. Although there are several interesting candidate channels that can form an amiloride/gadolinium-blockable channel, including some members of the DEG/ENac, ASIC, and TRP channel families (Waldmann and Lazdunski, 1998; Price et al., 2000; Delmas, 2004; McIlwrath et al., 2005; Hu et al., 2006; Kwan et al., 2006), it is not yet clear which channels form the core mechanosensory apparatus in both low- and high-threshold mechanoreceptors.

We thank A. Fernandez for expert technical assistance and N. Osorio and F. Padilla for reading earlier versions of the manuscript.

This work was supported by the Centre National de la Recherche Scientifique (CNRS) and by grants from the Agence Nationale de la Recherche (ANR-05-NEUR-031), the ARC-INCa-2006, and the French Research Ministry (ACI BCMS).

Olaf S. Andersen served as editor.

Submitted: 14 September 2006
Accepted: 4 December 2006

REFERENCES

Akaike, N., P.G. Kostyuk, and Y.V. Osipchuk. 1989. Dihydropyridine-sensitive low-threshold calcium channels in isolated rat hypothalamic neurones. *J. Physiol.* 412:181–195.

Akopian, A.N., L. Sivilotti, and J.N. Wood. 1996. A tetrodotoxin-resistant voltage-gated sodium channel expressed by sensory neurons. *Nature.* 379:257–262.

Anderberg, M.R. 1973. Cluster Analysis for Applications. Academic Press, New York. 359 pp.

Backx, P.H., D.T. Yue, J.H. Lawrence, E. Marban, and G.F. Tomaselli. 1992. Molecular localization of an ion-binding site within the pore of mammalian sodium channels. *Science.* 257:248–251.

Baker, M.D., S.Y. Chandra, Y. Ding, S.G. Waxman, and J.N. Wood. 2003. GTP-induced tetrodotoxin-resistant Na^+ current regulates excitability in mouse and rat small diameter sensory neurones. *J. Physiol.* 548:373–382.

Bautista, D.M., S.E. Jordt, T. Nikai, P.R. Tsuruda, A.J. Read, J. Poblete, E.N. Yamoah, A.I. Basbaum, and D. Julius. 2006. TRPA1 mediates the inflammatory actions of environmental irritants and proalgesic agents. *Cell.* 124:1269–1282.

Benn, S.C., M. Costigan, S. Tate, M. Fitzgerald, and C.J. Woolf. 2001. Developmental expression of the TTX-resistant voltage-gated sodium channels Nav1.8 (SNS) and Nav1.9 (SNS2) in primary sensory neurons. *J. Neurosci.* 21:6077–6085.

Birder, L.A., and E.R. Perl. 1994. Cutaneous sensory receptors. *J. Clin. Neurophysiol.* 11:534–552.

Blair, N.T., and B.P. Bean. 2002. Roles of tetrodotoxin (TTX)-sensitive Na^+ current, TTX-resistant Na^+ current, and Ca^{2+} current in the action potentials of nociceptive sensory neurons. *J. Neurosci.* 22:10277–10290.

Bossu, J.L., A. Feltz, and J.M. Thomann. 1985. Depolarization elicits two distinct calcium currents in vertebrate sensory neurones. *Pflugers Arch.* 403:360–368.

Bourinet, E., A. Alloui, A. Monteil, C. Barrere, B. Couette, O. Poirot, A. Pages, J. McRory, T.P. Snutch, A. Eschalier, and J. Nargeot. 2005. Silencing of the Cav3.2 T-type calcium channel gene in sensory neurons demonstrates its major role in nociception. *EMBO J.* 24:315–324.

Carbone, E., and H.D. Lux. 1984. A low voltage-activated, fully inactivating Ca channel in vertebrate sensory neurones. *Nature.* 310:501–502.

Cardenas, C.G., L.P. Del Mar, and R.S. Scroggs. 1995. Variation in serotonergic inhibition of calcium channel currents in four types of rat sensory neurons differentiated by membrane properties. *J. Neurophysiol.* 74:1870–1879.

Caterina, M.J., and D. Julius. 2001. The vanilloid receptor: a molecular gateway to the pain pathway. *Annu. Rev. Neurosci.* 24:487–517.

Clozel, J.P., E.A. Ertel, and S.I. Ertel. 1997. Discovery and main pharmacological properties of mibefradil (Ro 40-5967), the first selective T-type calcium channel blocker. *J. Hypertens. Suppl.* 15:S17–S25.

Coste, B., N. Osorio, F. Padilla, M. Crest, and P. Delmas. 2004. Gating and modulation of presumptive $Na_V1.9$ channels in enteric and spinal sensory neurons. *Mol. Cell. Neurosci.* 26:123–134.

Cribbs, L.L., J.H. Lee, J. Yang, J. Satin, Y. Zhang, A. Daud, J. Barclay, M.P. Williamson, M. Fox, M. Rees, and E. Perez-Reyes. 1998. Cloning and characterization of α1H from human heart, a member of the T-type Ca^{2+} channel gene family. *Circ. Res.* 83:103–109.

Cummins, T.R., S.D. Dib-Hajj, J.A. Black, A.N. Akopian, J.N. Wood, and S.G. Waxman. 1999. A novel persistent tetrodotoxin-resistant sodium current in SNS-null and wild-type small primary sensory neurons. *J. Neurosci.* 19:RC43.

Delmas, P. 2004. Polycystins: from mechanosensation to gene regulation. *Cell.* 118:145–148.

Delmas, P., F.C. Abogadie, N.J. Buckley, and D.A. Brown. 2000. Calcium channel gating and modulation by transmitters depend on cellular compartmentalization. *Nat. Neurosci.* 3:670–678.

Dib-Hajj, S.D., L. Tyrrell, J.A. Black, and S.G. Waxman. 1998. NaN, a novel voltage-gated Na channel, is expressed preferentially in peripheral sensory neurons and down-regulated after axotomy. *Proc. Natl. Acad. Sci. USA.* 95:8963–8968.

Djouhri, L., L. Bleazard, and S.N. Lawson. 1998. Association of somatic action potential shape with sensory receptive properties in guinea-pig dorsal root ganglion neurones. *J. Physiol.* 513:857–872.

Dogrul, A., L.R. Gardell, M.H. Ossipov, F.C. Tulunay, J. Lai, and F. Porreca. 2003. Reversal of experimental neuropathic pain by T-type calcium channel blockers. *Pain.* 105:159–168.

Drew, L.J., J.N. Wood, and P. Cesare. 2002. Distinct mechanosensitive properties of capsaicin-sensitive and -insensitive sensory neurons. *J. Neurosci.* 22:RC228.

Drew, L.J., D.K. Rohrer, M.P. Price, K.E. Blaver, D.A. Cockayne, P. Cesare, and J.N. Wood. 2004. Acid-sensing ion channels ASIC2 and ASIC3 do not contribute to mechanically activated currents in mammalian sensory neurones. *J. Physiol.* 556:691–710.

Dubreuil, A.S., H. Boukhaddaoui, G. Desmadryl, C. Martinez-Salgado, R. Moshourab, G.R. Lewin, P. Carroll, J. Valmier, and

F. Scamps. 2004. Role of T-type calcium current in identified D-hair mechanoreceptor neurons studied in vitro. *J. Neurosci.* 24:8480–8484.

Fang, X., L. Djouhri, J.A. Black, S.D. Dib-Hajj, S.G. Waxman, and S.N. Lawson. 2002. The presence and role of the tetrodotoxin-resistant sodium channel Na(v)1.9 (NaN) in nociceptive primary afferent neurons. *J. Neurosci.* 22:7425–7433.

Fang, X., S. McMullan, S.N. Lawson, and L. Djouhri. 2005. Electrophysiological differences between nociceptive and non-nociceptive dorsal root ganglion neurones in the rat in vivo. *J. Physiol.* 565:927–943.

Fang, X., L. Djouhri, S. McMullan, C. Berry, S.G. Waxman, K. Okuse, and S.N. Lawson. 2006. Intense isolectin-B4 binding in rat dorsal root ganglion neurons distinguishes C-fiber nociceptors with broad action potentials and high Nav1.9 expression. *J. Neurosci.* 26:7281–7292.

Fox, A.P., M.C. Nowycky, and R.W. Tsien. 1987. Single-channel recordings of three types of calcium channels in chick sensory neurones. *J. Physiol.* 394:173–200.

Gomora, J.C., J. Murbartian, J.M. Arias, J.H. Lee, and E. Perez-Reyes. 2002. Cloning and expression of the human T-type channel Ca(v)3.3: insights into prepulse facilitation. *Biophys. J.* 83:229–241.

Herrington, J., and C.J. Lingle. 1992. Kinetic and pharmacological properties of low voltage-activated Ca^{2+} current in rat clonal (GH3) pituitary cells. *J. Neurophysiol.* 68:213–232.

Herzog, R.I., T.R. Cummins, and S.G. Waxman. 2001. Persistent TTX-resistant Na^+ current affects resting potential and response to depolarization in simulated spinal sensory neurons. *J. Neurophysiol.* 86:1351–1364.

Hu, J., N. Milenkovic, and G.R. Lewin. 2006. The high threshold mechanotransducer: a status report. *Pain.* 120:3–7.

Huguenard, J.R. 1996. Low-threshold calcium currents in central nervous system neurons. *Annu. Rev. Physiol.* 58:329–348.

Kim, D., I. Song, S. Keum, T. Lee, M.J. Jeong, S.S. Kim, M.W. McEnery, and H.S. Shin. 2001. Lack of the burst firing of thalamocortical relay neurons and resistance to absence seizures in mice lacking α1G T-type Ca^{2+} channels. *Neuron.* 31:35–45.

Kobayashi, K., T. Fukuoka, K. Obata, H. Yamanaka, Y. Dai, A. Tokunaga, and K. Noguchi. 2005. Distinct expression of TRPM8, TRPA1, and TRPV1 mRNAs in rat primary afferent neurons with adelta/c-fibers and colocalization with trk receptors. *J. Comp. Neurol.* 493:596–606.

Kostyuk, P.G., O.A. Krishtal, and V.I. Pidoplichko. 1975. Effect of internal fluoride and phosphate on membrane currents during intracellular dialysis of nerve cells. *Nature.* 257:691–693.

Kuo, C.C., T.J. Lin, and C.P. Hsieh. 2002. Effect of Na^+ flow on Cd^{2+} block of tetrodotoxin-resistant Na^+ channels. *J. Gen. Physiol.* 120:159–172.

Kuo, C.C., W.Y. Chen, and Y.C. Yang. 2004. Block of tetrodotoxin-resistant Na^+ channel pore by multivalent cations: gating modification and Na^+ flow dependence. *J. Gen. Physiol.* 124:27–42.

Kwan, K.Y., A.J. Allchorne, M.A. Vollrath, A.P. Christensen, D.S. Zhang, C.J. Woolf, and D.P. Corey. 2006. TRPA1 contributes to cold, mechanical, and chemical nociception but is not essential for hair-cell transduction. *Neuron.* 50:277–289.

Lawson, S.N. 2002. Phenotype and function of somatic primary afferent nociceptive neurones with C-, Aδ- or Aα/β-fibres. *Exp. Physiol.* 87:239–244.

Lee, J.H., A.N. Daud, L.L. Cribbs, A.E. Lacerda, A. Pereverzev, U. Klockner, T. Schneider, and E. Perez-Reyes. 1999. Cloning and expression of a novel member of the low voltage-activated T-type calcium channel family. *J. Neurosci.* 19:1912–1921.

Leffler, A., R.I. Herzog, S.D. Dib-Hajj, S.G. Waxman, and T.R. Cummins. 2005. Pharmacological properties of neuronal TTX-resistant sodium channels and the role of a critical serine pore residue. *Pflugers Arch.* 451:454–463.

Lewin, G.R., and R. Moshourab. 2004. Mechanosensation and pain. *J. Neurobiol.* 61:30–44.

Martin, R.L., J.H. Lee, L.L. Cribbs, E. Perez-Reyes, and D.A. Hanck. 2000. Mibefradil block of cloned T-type calcium channels. *J. Pharmacol. Exp. Ther.* 295:302–308.

Maruyama, H., M. Yamamoto, T. Matsutomi, T. Zheng, Y. Nakata, J.N. Wood, and N. Ogata. 2004. Electrophysiological characterization of the tetrodotoxin-resistant Na^+ channel, Na(v)1.9, in mouse dorsal root ganglion neurons. *Pflugers Arch.* 449:76–87.

McCarter, G.C., D.B. Reichling, and J.D. Levine. 1999. Mechanical transduction by rat dorsal root ganglion neurons in vitro. *Neurosci. Lett.* 273:179–182.

McIlwrath, S.L., J. Hu, G. Anirudhan, J.B. Shin, and G.R. Lewin. 2005. The sensory mechanotransduction ion channel ASIC2 (acid sensitive ion channel 2) is regulated by neurotrophin availability. *Neuroscience.* 131:499–511.

McNulty, M.M., and D.A. Hanck. 2004. State-dependent mibefradil block of Na^+ channels. *Mol. Pharmacol.* 66:1652–s1661.

Nelson, M.T., P.M. Joksovic, E. Perez-Reyes, and S.M. Todorovic. 2005. The endogenous redox agent L-cysteine induces T-type Ca^{2+} channel-dependent sensitization of a novel subpopulation of rat peripheral nociceptors. *J. Neurosci.* 25:8766–8775.

Nowycky, M.C., A.P. Fox, and R.W. Tsien. 1985. Three types of neuronal calcium channel with different calcium agonist sensitivity. *Nature.* 316:440–443.

Perez-Reyes, E. 2003. Molecular physiology of low-voltage-activated t-type calcium channels. *Physiol. Rev.* 83:117–161.

Perez-Reyes, E., L.L. Cribbs, A. Daud, A.E. Lacerda, J. Barclay, M.P. Williamson, M. Fox, M. Rees, and J.H. Lee. 1998. Molecular characterization of a neuronal low-voltage-activated T-type calcium channel. *Nature.* 391:896–900.

Petruska, J.C., J. Napaporn, R.D. Johnson, J.G. Gu, and B.Y. Cooper. 2000. Subclassified acutely dissociated cells of rat DRG: histochemistry and patterns of capsaicin-, proton-, and ATP-activated currents. *J. Neurophysiol.* 84:2365–2379.

Petruska, J.C., J. Napaporn, R.D. Johnson, and B.Y. Cooper. 2002. Chemical responsiveness and histochemical phenotype of electrophysiologically classified cells of the adult rat dorsal root ganglion. *Neuroscience.* 115:15–30.

Price, M.P., G.R. Lewin, S.L. McIlwrath, C. Cheng, J. Xie, P.A. Heppenstall, C.L. Stucky, A.G. Mannsfeldt, T.J. Brennan, H.A. Drummond, et al. 2000. The mammalian sodium channel BNC1 is required for normal touch sensation. *Nature.* 407:1007–1011.

Priest, B.T., B.A. Murphy, J.A. Lindia, C. Diaz, C. Abbadie, A.M. Ritter, P. Liberator, L.M. Iyer, S.F. Kash, M.G. Kohler, et al. 2005. Contribution of the tetrodotoxin-resistant voltage-gated sodium channel $Na_V1.9$ to sensory transmission and nociceptive behavior. *Proc. Natl. Acad. Sci. USA.* 102:9382–9387.

Rush, A.M., M.E. Brau, A.A. Elliott, and J.R. Elliott. 1998. Electrophysiological properties of sodium current subtypes in small cells from adult rat dorsal root ganglia. *J. Physiol.* 511:771–789.

Sangameswaran, L., S.G. Delgado, L.M. Fish, B.D. Koch, L.B. Jakeman, G.R. Stewart, P. Sze, J.C. Hunter, R.M. Eglen, and R.C. Herman. 1996. Structure and function of a novel voltage-gated, tetrodotoxin-resistant sodium channel specific to sensory neurons. *J. Biol. Chem.* 271:5953–5956.

Scroggs, R.S., and A.P. Fox. 1992. Calcium current variation between acutely isolated adult rat dorsal root ganglion neurons of different size. *J. Physiol.* 445:639–658.

Sheets, M.F., and D.A. Hanck. 1992. Mechanisms of extracellular divalent and trivalent cation block of the sodium current in canine cardiac Purkinje cells. *J. Physiol.* 454:299–320.

Shin, J.B., C. Martinez-Salgado, P.A. Heppenstall, and G.R. Lewin. 2003. A T-type calcium channel required for normal function of a mammalian mechanoreceptor. *Nat. Neurosci.* 6:724–730.

Talley, E.M., L.L. Cribbs, J.H. Lee, A. Daud, E. Perez-Reyes, and D.A. Bayliss. 1999. Differential distribution of three members of a gene family encoding low voltage-activated (T-type) calcium channels. *J. Neurosci.* 19:1895–1911.

Tang, C.M., F. Presser, and M. Morad. 1988. Amiloride selectively blocks the low threshold (T) calcium channel. *Science.* 240:213–215.

Tate, S., S. Benn, C. Hick, D. Trezise, V. John, R.J. Mannion, M. Costigan, C. Plumpton, D. Grose, Z. Gladwell, et al. 1998. Two sodium channels contribute to the TTX-R sodium current in primary sensory neurons. *Nat. Neurosci.* 1:653–655.

Todorovic, S.M., and C.J. Lingle. 1998. Pharmacological properties of T-type Ca^{2+} current in adult rat sensory neurons: effects of anticonvulsant and anesthetic agents. *J. Neurophysiol.* 79:240–252.

Todorovic, S.M., A. Meyenburg, and V. Jevtovic-Todorovic. 2002. Mechanical and thermal antinociception in rats following systemic administration of mibefradil, a T-type calcium channel blocker. *Brain Res.* 951:336–340.

Visentin, S., A. Zaza, A. Ferroni, C. Tromba, and C. DiFrancesco. 1990. Sodium current block caused by group IIb cations in calf Purkinje fibres and in guinea-pig ventricular myocytes. *Pflugers Arch.* 417:213–222.

Waldmann, R., and M. Lazdunski. 1998. H^+-gated cation channels: neuronal acid sensors in the NaC/DEG family of ion channels. *Curr. Opin. Neurobiol.* 8:418–424.

Wang, H. and C.J. Woolf. 2005. Pain TRPs. *Neuron.* 46:9–12.

Waxman, S.G., S. Dib-Hajj, T.R. Cummins, and J.A. Black. 1999. Sodium channels and pain. *Proc. Natl. Acad. Sci. USA.* 96:7635–7639.

White, G., D.M. Lovinger, and F.F. Weight. 1989. Transient low-threshold Ca^{2+} current triggers burst firing through an afterdepolarizing potential in an adult mammalian neuron. *Proc. Natl. Acad. Sci. USA.* 86:6802–6806.

Wood, J.N., J.P. Boorman, K. Okuse, and M.D. Baker. 2004. Voltage-gated sodium channels and pain pathways. *J. Neurobiol.* 61:55–71.